Response to reviewer's comments

Anonymous Referee #1:

General comments:

The manuscript discusses a pollution event that produced a "haze front" over Beijing, China on 24 December 2015. The haze front is a sharp change in visibility on the boundary of warm dry clean air meeting cool moist polluted air over the city. The warm air mass was created by a foehn wind blowing down from the mountains to the north and west of Beijing. The interaction between the two air masses is analysed in detail using meteorological variables, and particular matter measurements from a number of sites across the city. The authors then conclude with statistics of how often this sort of event occurs. These events can have a large impact on air quality in Beijing and can potentially be applied to other cities with a similar geographical layout. I am not aware of a similar publication into haze fronts caused by foehn winds. The manuscript reads well and the English is good, but there are some sections that need changing. Great use of many different measurement platforms. As there are a lot of sites, Table 1 and the map in Figure 1 really help for orientation. But some of the figures need some work (see below). The supplemental figures are helpful for providing a broader picture.

We sincerely thank the reviewer for in-depth comments and helpful suggestions. We have responded to all the comments point-by-point and made corresponding changes in the manuscript. Following are detailed responses to all the comments.

I could not find a video (mentioned during the submission).

We are very sorry for forgetting to upload the video during the submission. This video will be submitted as a supplement along with the revised manuscript.

Specific comments:

Define the time zone LST (I assume it's local time)

The time zone LST (Local Standard Time) is Beijing time. We have defined the time zone LST in the manuscript.

PM2.5: sometimes the 2.5 is subscript or normal script

Thank you. All of 2.5 in PM2.5 have been set as subscripts in the manuscript.

Mini-MPL: sometimes you refer to the Mini-MPL as Min-MPL

Thank you. All 'Min-MPL' has been changed to 'Mini-MPL'.

Table 1:

- observation heights missing

Thank you. This has been corrected.

- AOT AWS is missing

Thank you. This has been corrected.

Section 3.1 needs to discuss the meteorological conditions in a bit more detail.

- You show a number of weather charts, but don't really explain what the relevance is to the haze front case study. The upper level trough is not really relevant here.

Thank you. We have added more explanations to this section. We also have adjusted the sequence of Section 3.1 as Referee #2 suggested. In brief, the upper air flows were dominated by northwesterly winds. And before the impact of the synoptic system, surface winds were weak. This synoptic pattern was one of typically frequent unfavorable conditions which exacerbate air pollution.

- You don't reference the 850 mb charts in the main text. What height is the 850 mb surface? This is useful when comparing to the wind profiler data (Fig. 2d). But ultimately the surface wind is weak and doesn't really correlate with the upper level data in the morning. Figure 10 also shows very low wind speeds in the morning before the foehn arrives. Looking at Figure S1a there doesn't seem to be any evidence of a cold front or dominant wind direction.

The height of 850 mb at Beijing is ~ 1500 m above the ground level. The winds at this height in Figure 2d agree well with the winds at same height in Figure 3c and 3d. We agree with you that the cold front marked in Figure 3e, which was automatically plotted by the software, seems not obvious and unwarranted. Therefore, we have re-plotted the map without the cold front.

- Figure 3: if possible add some dots to show measurement sites if they are not too close together. Maybe same as Figure 4 (IUM, IAP and GXT). As a minimum a dot showing the centre of Beijing.

Thank you for the comment. It is hard to distinguish sites in such small maps. So we have made the boundaries of Beijing bold and brown on the maps.

Also, in the caption it should be '850 mb'.

The caption has been corrected.

- Line 158 says the flow is weak south-westerly in Figure 2c, but looks weak northeasterly to me in Figure 3f. Which one is it?

The flow is southwesterly in Figure 3f. Please see an enlarged figure below. The black dot pointed by a red arrow is the GXT site with ~ 1 m/s southwesterly surface wind.

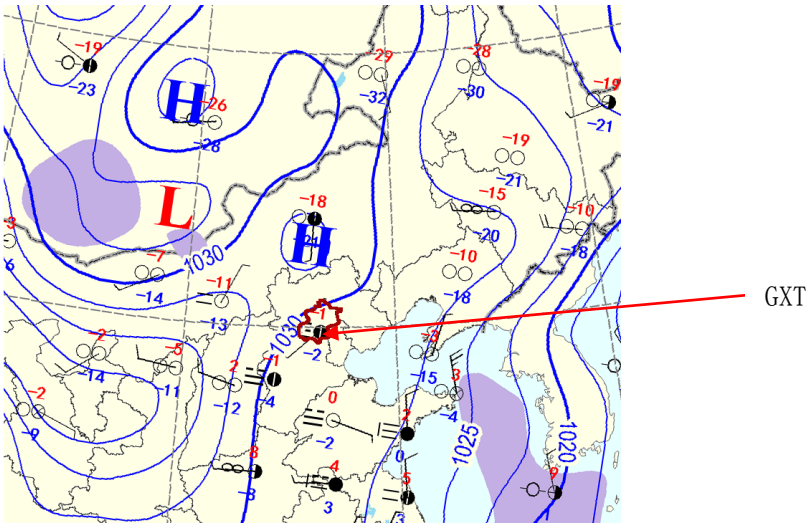

- The radiosonde profile in Figure 2c also shows up the vertical extent of the haze front at GXT nicely.

Thank you for the comment.

- Figure 2a: Is it possible to add some sort of distribution of hourly PM2.5 values from the different sites (percentiles)? The event is highly variable.

We are not sure about how to plot the percentiles in Figure 2. An alternative way is to plot hourly PM2.5 value for all three representative sites and three-sites mean value. Please see the new Figure 2a.

Also, what area does the average PM2.5 cover?

The average PM2.5 is the mean PM2.5 concentration of 35 sites in Beijing shown on the below site map and the new Figure 1a. Most of the sites are located in plain areas in Beijing.

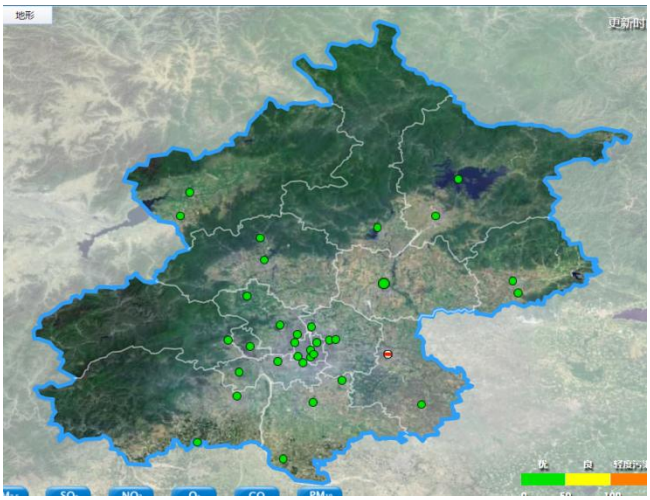

Source: http://zx.bjmemc.com.cn/getAqiList.shtml?timestamp=1601452931296

Section 3.2:

- Figure 4: it might help to add a narrow line to the images where you can pick out the haze front as it is quite difficult to see at first (similar to Figure 6)

Thank you for the comment. We have added red lines to illustrate the haze front in Figure 4.

- Figure 5b: The text says that the wind direction changes suddenly at t2 (ie. 16:21 LST) (line 177) but I can't see this in the figure. Are the wind directions in the plot correct?

The wind directions in the plot are correct. As a result of using wind data observed at Chedougou (CDG) site, ~ 1 km north of the IUM, the wind direction changes at CDG didn't match the PM2.5 concentration changes at IUM very well. In fact, there is an AWS collocated with the Mini-MPL at the top of the IUM building, which observed wind direction and wind speed but with more missing data during the HF passing period. We used wind direction and wind speed data at IUM and redrew the Figure 5b. Besides the wind data observed at the IUM site, you can also find the wind direction changes agreed well with the PM2.5 concentration changes from the supplemental video.

- Figure 5 (caption, line 673): The scanning lidar is at IUM not IAP.

Thank you. This has been corrected.

- Figure 7: can you add the haze front line to this plot? Also, personal preference: maybe flip the colour bar (red as dry and blue as moist)

Thank you for the comment. We have added the haze front line to Figure 7, and flipped the color bar as you suggested.

- line 193: revise the word "surrounded"

Thank you for the comment. We have revised the word "surrounded". The sentence now reads:

"The foehn winds with the warm, dry, and clean air collided with more southerly or southeasterly winds with the cold, wet, and polluted air and resulted in oscillations of the HF line (Fig. 6-7)."

Section 3.3:

- Figure 8 has values every hour and not three-hourly as mentioned in the caption. The use of tendency is a bit confusing. Using it for pressure works, to show the small differences between sites that produce the pressure gradient. Are the tendencies subtracted from the mean of the whole day? Unless the absolute values of temperature and humidity for the different sites are very different, I would find it easier if they were absolute (or at least include the mean values in the plot eg. Tmean[CP]=x.xdegC) as you reference absolute values in the main text.

Thank you for the comment. The pressure tendency we used here is defined as P_{t0}-P_{t0-3}, where P_{t0} is the pressure at t0 (current time in hour) and P_{t0-3} is the pressure at 3 hours before t0. A similar tendency definition was used for the temperature and specific humidity. We agree with your comment that the use of tendency is a bit confusing. Hence, we have re-plotted Figure 8a, 8b and 8c by using the half-hourly pressure anomaly, temperature and specific humidity, respectively. We have marked the time of HF passage at CDG in Figure 8 as Refree #2 suggested. Also, we have revised sentences related to the changes in Figure 8.

- line 223: I think “gusty the foehn” should be “the gusty foehn”.

Thank you. This has been corrected.

Also, what do you mean by “enlarging the coverage”?

By “enlarging the coverage”, we mean to express the enlarged scope or coverage of the UHI after the warm-dry air mass driven by the gusty foehn merged with the UHI.

- line 225: do you mean “the pressure increased significantly compared to the other sites”?

We meant the pressure increased significantly when the haze front passed over the CDG site. But because we modified Figure 8 and found the pressure only increased slightly, we have revised the sentence. It now reads:

“When the HF passed over CDG, the humidity and PM2.5 concentrations significantly increased, the pressure slightly increased, but the temperature slightly decreased (Fig. 8).”

- line 229: Reference that it is IAP Doppler lidar data in the text to make it clear. Otherwise I have to look at the figure to work that out.

Thank you for the comment. We have revised the sentence. The sentence now reads:

“At IAP around noon, the Doppler lidar detected a northwesterly wind and a significantly increased updraft between 450 m and 1250 m height above the surface, and the wind direction below 500 m changed from northeast to northwest (Fig. 9).”

- line 233: Please reword. I think you mean something like: “the temperature was higher and the turbulence was increased mainly between 12:00 LST and 19:00 LST”. The current wording implies that it started low at 12:00 LST and increased steadily to a maximum at 19:00 LST.

Thank you. We have reworded the sentence.

- line 236 and Figure 10: you might benefit from including potential temperature here, as this shows up stability better.

Thank you for the comment. But there are no pressure observations at 15 levels on the IAP tower.

- line 237: Looks like the enhanced pollution wasn’t just below 100 meters. Figure 9 suggests the aerosol went all the way up to 400 meters.

Thank you. We reworded the sentence. The sentence now reads:

“The boundary layer became more stably stratified near the surface, leading to enhanced pollution in the lowest few hundred meters.”

- Figure 11: Are the tower plots correct? I’d expect DR to decrease as you get closer to the ground, but 47 m shows the highest DR.

Thank you for the comment. The tower plots are correct.

The reason that the DR at 47 m is highest is due to the ‘canyon trapping’ effect on shortwave radiation in the urban canopy layer (Oke, 2017). The rugosity of the urban surface contributes to the lower albedo values at higher solar elevation angles as more short-wave radiation enters

the street canyons where it is trapped (Christen and Vogt, 2004; Kotthaus and Grimmond, C.S.B., 2013). The IAP tower is surrounded by 4- to 20-story buildings with heights of 10 to 60 m (Liu et al., 2017; Wang et al., 2019). Some buildings just south of the IAP tower are higher than the pyrgeometers and pyranometers mounted at 47 m on the tower causing the additional shortwave radiation trapping in the street canyon, especially when solar elevation angles are greater (Dou et al., 2018).

Also, it might be easier to read if you list the tower levels in one column in the legend.

Thank you for the comment. We have listed the tower levels in one column in the legend.

- line 240 and Figure 11: do you mean AOT instead of ATZX?

Thank you. Yes. We have changed all "ATZX" into "AOT".

- line 243: The lower PBL height is also to do with the PBL height being suppressed by the overrunning foehn wind, not just the reduced solar radiation at the ground.

Thank you for the comment. According to our observational analysis, there is no evidence that foehn winds affected GXT. Please see in Figure S2a the southern most areas that foehn winds have invaded. Hence, the lower PBL height at GXT is mainly due to less solar radiation and less turbulence, and positive feedback between the PBL height and the aerosol concentration.

Section 4:

- line 302: are mountain-plains winds and mountain breezes the same thing?

Mountain breezes are a part of mountain and valley breezes that refer to the cooler, more-dense air that glides downslope into the valley during nighttime (Ahrens, 2003). Mountain-plain winds result from horizontal temperature differences between the air over a mountain massif and the air over the surrounding plains, producing large-scale winds that blow up or down the outer slopes of a mountain massif (Whiteman, 2000). The scale of mountain-plain winds is larger than the scale of mountain breezes.

- line 319: add the types in brackets (eg. '(Type A)') to the main text to make it more clear.

Thank you. We have reworded the sentences.

- Table 2: rewording for the types: eg. "Type A: polluted cases where PM2.5 concentrations for the CP, AOT and YZ sites had decreased 24 hours after the foehn's occurrence."

Thank you for the comment. We have reworded the table note.

Data availability: Couldn't access http://www.ium.cn/dataCenter/ (Page not found)

Sorry about the invalid link. The link of the datacenter of IUM has been changed into http://www.ium.cn:8088/ in 2020.

Couldn't access http://106.37.208.233:20035/ (Couldn't install Silverlight on my system)

Please visit https://quotsoft.net/air/ where the PM2.5 data sources from the China Environmental Monitoring Station and the Beijing Environmental Protection Testing Center.

References for review replies:

Ahrens C. D.: Meteorology Today: An Introduction to Weather, Climate and the Environment. Thomson Learning, USA, 2003.

Christen, A., Vogt, R.: Energy and radiation balance of a Central European City. Int. J. Climatol. 24, 1395–1421, 2004.

Dou J, Grimmond S, Cheng Z, Miao S, Feng D, Liao M: Summertime surface energy balance fluxes at two Beijing sites. IntJ Climatol., 39, 2793–2810, https://doi.org/10.1002/joc.5989, 2019.

Kotthaus, S., Grimmond, C.S.B. Energy exchange in a dense urban environment – Part II: Impact of spatial heterogeneity of the surface. Urban Climate, 10, 261-280, http://dx.doi.org/10.1016/j.uclim.2013.10.001, 2013.

Liu, J. K., Gao, Z. Q., Wang, L. L., Li, Y. B., and Gao, C. Y.: The impact of urbanization on wind speed and surface aerodynamic characteristics in Beijing during 1991–2011, Meteorol. Atmos. Phys., 130, 311–324, https://doi.org/10.1007/s00703-017-0519-8, 2017.

Oke, T.R., Mills, G., Christen, A. and Voogt, J.A.: Urban Climates. Cambridge: Cambridge University Press, 525 pp. https://doi.org/10.1017/9781139016476, 2017.

Wang, L., Liu, J., Gao, Z., Li, Y., Huang, M., Fan, S., Zhang, X., Yang, Y., Miao, S., Zou, H., Sun, Y., Chen, Y., and Yang, T.: Vertical observations of the atmospheric boundary layer structure over Beijing urban area during air pollution episodes, Atmos. Chem. Phys., 19, 6949–6967, https://doi.org/10.5194/acp-19-6949-2019, 2019.

Whiteman, C. D.: Mountain Meteorology: Fundamentals and Applications, Oxford Univ. Press, New York, 2000.

Response to reviewer's comments

Anonymous Referee #2:

This observational study describes the evolution of meteorological conditions and PM concentrations associated with a foehn event. As the warm, dry, and relatively clean foehn wind meets the cold, wet and polluted air mass in the Beijing area, a haze front formed. The large observational network captured the characteristics and evolution of this haze front as it moved through the network. The level of details captured by both the ground and the upper air observations (including wind profilers, Doppler Lidars and radiosounds) makes this study a useful contribution to the literature regarding foehn characteristics and its influence on air pollution.

The manuscript contains a large number of figures that are generally in good quality. The writing, however, could use substantial improvements, as described below.

We sincerely thank the reviewer for in-depth comments and helpful suggestions. We have responded to all the comments point-by-point and made corresponding changes in the manuscript. Following are detailed responses to all the comments.

Define the key terms. The central focus of the manuscript is on haze front, but there is no clear definition on what a haze front is and how to identify it from the observations. It is stated in the paper that "The HF line was identified by temperature and humidity contrasts between the warm and cold air masses and the convergence line of the surface wind field". How does this differ from foehn front? Is HF the same as foehn front? I would expect that a HZ should be identified by sharp contrast in PM values, instead of temperature and humidity. If HZ and foehn front are the same, then say it. In sum, it should be clearly stated near the beginning what you mean by haze front, foehn front, and what criteria are used to identify these fronts from your observational data.

Thank you for the comment. A haze front is not the same as a foehn front, but has some similarity to a foehn front in some cases, like in the case we studied here. "The haze front" is denoted mainly by its front-like structure and sharp contrast in polluted aerosol. This is why we didn't use the name "foehn front" in the manuscript. The foehn front is basically the foehn-induced "minifront" phenomena described in the literature by Vergeiner (2004) and Li et al. (2015). We identify a haze front by sharp contrast in PM values, instead of temperature and humidity. Thus, we have stated the meaning of the haze front in the introduction. The new added sentence reads:

"This HF was identified by a sharp contrast in $PM_{2.5}$ concentration and a convergence line in the surface wind field."

We also have revised the sentence you quoted above. The sentence now reads:

"The HF line was identified by a sharp contrast in $PM_{2.5}$ concentration, temperature and humidity between the warm and cold air masses and the convergence line of the surface wind field (Fig. 6-7, Fig. S1-S3), which was also consistent with the front edge of the hazy air mass seen in the satellite images (Fig. 4)."

The manuscript could benefit from reorganization. It is good to begin with describing

background conditions for this episode. The sequence of the current description is: PM time series, sounding profiles, profiler winds, and finally synoptic patterns. I would reverse the order, starting from synoptic patterns and ending with surface observations including PM time series. More details are needed in the description of synoptic conditions. Right now, the synoptic patterns are shown, but there is very little discussion. In addition to describing the synoptic patterns for this case, there should be some discussion on how typical the pattern is and how often it occurs in order to put this particularly episode into historical context.

Thank you for the comment. We have adjusted the sequence of Section 3.1 as you suggested. Also, we have added more description of synoptic conditions in this section, and compared this synoptic pattern with the statistics of unfavorable synoptic conditions which exacerbate air pollution (Wang et al., 2020).

Further, I do not see the need to separate "The evolution of HF "and "Characteristics of the HF and foehn winds" into two sections.

Thank you for the comment. We have combined the section "3.2 The evolution of HF" and the section "3.3 Characteristics of the HF and foehn winds" into one section, named "3.2 The evolution and characteristics of the HF and foehn winds".

Some of the discussion could be improved. Some of the discussion is rather confusion. For example, "This HF occurred on 24 December 2015 concurrent with a severe air pollution episode." But according to the PM time series in Fig. 2a, PM is high on the 23rd, but dropped down to nearly 100 on the morning of the 24th, and gradually increased to nearly 500 in the afternoon of 25. So if HF occurred on the 24th, then it was not concurrent with severe air pollution episode. In fact, in the next paragraph, it is mentioned that "the Beijing area was clear with low pollution." It is unclear what the background pollution level was and what was associated by HF. Is the increase on the 24th due to the passage of HF? I would expect a sharp increase instead of a gradual increase.

Thank you for the comment. Because of using the mean $PM_{2.5}$ concentration of 35 sites in Beijing in Figure 2a, it is hard to distinguish the highly varied air pollution on 24th. So we have replaced Figure 2a with a new figure using hourly-mean $PM_{2.5}$ concentration of CP, AOT, YZ and 3-stations mean. According to the new Figure 2a, the Beijing area was clear with low pollution on the morning of the 24th, which was also verified from satellite images (Figure 4a, 4b). In brief, the background pollution level was low in Beijing before the passage of the HF on the 24th. The HF affected YZ causing a sharp increase in PM concentration at around noon. But meanwhile, $PM_{2.5}$ concentration decreased inversely at CP and kept a very low level at AOT. When the HZ arrived at AOT at 22:00 LST, it caused a sharp increase in PM (increased 268 μg m^{-3} in one hour). Consequently, the PM increase on the 24th was mainly due to the passage of HF. We have rewritten this whole paragraph. The sentences now read:

"This HF occurred on 24 December 2015 after a severe air pollution event. The mean $PM_{2.5}$ concentrations of CP, AOT and YZ varied between 300-400 μg m^{-3} on the morning of 23 December, which is a severe Air Quality Index (AQI) pollution level (Fig. 2a). Thereafter, two significant $PM_{2.5}$ concentration decreases occurred around noon and midnight on that day.

During the day on 24 December, the mean $PM_{2.5}$ concentration decreased to 73 μg m^{-3} at 07:00 LST. At 11:00 LST, the $PM_{2.5}$ concentration at YZ sharply increased by 221 μg m^{-3} in one hour. At 13:00 LST, the $PM_{2.5}$ concentration at CP decreased from 112 μg m^{-3} to 32μg m^{-3}. The $PM_{2.5}$ concentration of AOT stayed below 80 μg m^{-3} until 22:00 LST when it sharply increased by 268 μg m^{-3} in one hour. The following day, the mean $PM_{2.5}$ concentration exceeded 500 μg m^{-3} at 14:00 LST."

In the discussion of satellite images, it is unclear how you distinguish haze from fog or clouds in the satellite images?

Thank you for the comment. We have rewritten the first sentence in the first paragraph of section 3.2. The sentences now read:

"The visible channel true color images from the Himawari satellite clearly showed the movement and evolution of the HF. Normally, on the true color satellite images, clouds look white and gray and tend to have texture; haze is usually featureless and pale gray or a dingy white; fog looks similar to the color of clouds but without texture. However, clouds, fog, and haze are sometimes difficult to distinguish from satellite imagery. Hence, we referred to weather phenomena, visibility and $PM_{2.5}$ concentration observed by surface meteorological and air quality stations to distinguish them. A dense fog covered northeastern Tianjin and half of Xianghe county of Heibei Province at 08:00 LST (Fig. 4a)."

Some of the descriptions used present tense while others used past tense. Be consistent.

Thank you. We have revised present tense into past tense.

The discussion about the HF and foehn characteristics is exhaustion to read. Better rewriting is necessary to improve readability.

Thank you for the comment. We have rewritten the discussion about the HF and foehn characteristics.

Figures are generally in good quality, but figure captions could use more details. For example, the caption for Figure 1 should include a description of the different symbols, although they are described in the text. Also include AWS and PM stations in Figure 1.

Thank you for the comment. We have revised Figure 1 as you suggested.

The font size for the axis labels in the time series plots and some of text in the figures should be enlarged. They are currently too small to read unless the figures are enlarged by 200% (e.g., Fig. 10 c vertical axis, Fig. 10 b, the label for the color bar; Figure 2b).

Thank you for the comment. We have enlarged axis labels, color bar labels and some text in Figure 10 and Figure 2.

Clearly mark the time of HF passage on the time series plots.

Thank you for the comment. We have marked the time of HF passage on the time series plots.

References for review replies:

Li, X., Xia, X., Wang, L., Cai, R., Zhao, L., Feng, Z., Ren, Q., Zhao, K.: The role of foehn in the formation of heavy air pollution events in Urumqi, China. J. Geophys. Res. Atmos., 120, 5371–5384, https://doi.org/10.1002/2014jd022778, 2015.

Vergeiner, J. : South foehn studies and a new foehn classification scheme in theWipp and Inn Valley, PhD thesis, Univ. of Innsbruck, Austria, 2004.

Wang X, Zhang R: Effects of atmospheric circulations on the interannual variation in PM2.5 concentrations over the Beijing–Tianjin–Hebei region in 2013–2018. Atmos Chem Phys 2020, 20(13):7667-7682.

A foehn-induced haze front in Beijing: observations and implications

Ju Li[1*], Zhaobin Sun[1], Donald H. Lenschow[2], Mingyu Zhou[3], Youjun Dou[1], Zhigang Cheng[1], Yaoting Wang[1], Qingchun Li[1]

[1] Institute of Urban Meteorology, Beijing,China
[2] National Center for Atmospheric Research, Boulder, CO, USA
[3] National Marine Environment Forecast Center, Beijing, China

**Correspondence to*: Ju Li (jli@ium.cn)

Abstract. Despite frequent foehns in the Beijing-Tianjin-Hebei (BTH) region, there are only a few studies of their effects on air pollution in this region, or elsewhere. Here, we discuss a foehn-induced haze front (HF) event using observational data to document its structure and evolution. Using a dense network of comprehensive measurements in the BTH region, our analyses indicate that the foehn played an important role in the formation of the HF with significant impacts on air pollution. Northerly warm-dry foehn winds, with low particulate concentration in the northern area, collided with a cold-wet polluted air mass to the south and formed an HF in the urban area. The HF, which is associated with a surface wind convergence line and distinct contrasts of temperature~~s~~, humidity, and pollutant concentrations, resulted in an explosive growth of particulate concentration. As the plains-mountain wind circulation was overpowered by the foehn, a weak pressure gradient due to the different air densities between air masses was the main factor forcing advances of the polluted air mass into the clean air mass, resulting in severe air pollution over the main urban areas. Our results show that the foehn can affect air pollution through two effects: direct wind transport of air pollutants, and altering the air mass properties to inhibit boundary-layer growth and thus indirectly aggravating air pollution. This study highlights the need to further investigate the foehn and its impacts on air pollution in the BTH region.

1 Introduction

Air pollution issues in China have been widely discussed and studied in recent decades. The region encompassing Beijing City, Tianjin City, and Hebei province, i.e. the Beijing-Tianjin-Hebei (BTH) region, is one of most polluted areas in China and has a very high level of 2.5 μm diameter particles ($PM_{2.5}$) ~~particular matter of 2.5 μm diameter ($PM_{2.5}$)~~ (Han et al., 2014; Gao et al., 2015; Jiang et al., 2015a; Wang et al., 2015). Furthermore, severe haze events occur frequently in the BTH region, especially in autumn and winter (Wang et al., 2013; Sun et al., 2014; Sun et al., 2016; Zhang et al., 2015; Li et al., 2016; Li et al., 2017), and negatively affect human health (Guo et al., 2017). Stagnant weather conditions and large anthropogenic emissions in this region are the main reasons for ~~heavy~~ the severe haze and pollution (Zhao et al., 2013; Liu et al., 2013; Wang et al., 2013; Zhang et al., 2014; Zhang et al., 2015; Liu et al., 2017). Previous studies have shown feedbacks between aerosol and meteorological variables (e.g., Steiner et al., 2013; Tie et al., 2017; Huang et al., 2018; Li et al., 2018a; Wu et al., 2019). A high concentration of $PM_{2.5}$ can weaken turbulence (Ren et al., 2019) and enhance stability in the planetary boundary layer (PBL) resulting in decreased PBL height and consequently increased $PM_{2.5}$ concentrations (Su et al., 2018), i.e. a positive feedback between aerosols and PBL height (Petäjä et al., 2016). Liu et al. (2018) found another positive feedback: decreased PBL height can increase relative humidity (RH), and, in turn, enhance secondary aerosol (SA) formation and further enhance particulate concentration, weaken solar radiation, and further decrease PBL height.

During severe haze events in the BTH region, $PM_{2.5}$ concentrations can increase as much as 200 μg~~.~~ m^{-3} in several hours (Zhong et al., 2017). On the one hand, SA formation through aerosol hygroscopic growth is one of the main reasons causing this explosive growth of particular matter (Han et al., 2015; Sun et al., 2014; Chen et al., 2019). Huang et al. (2014), for example, found that severe haze pollution events were mostly the result of SA. On the other hand, vertical and horizontal transport can also produce an explosive growth of partic~~ular matter~~les. Observations have shown that downward transport by large coherent eddies also produced explosive growth of surface $PM_{2.5}$ concentrations (Han et al., 2018; Li et al., 2018b). Complex topography, land-use and land-cover, (~~,~~e.g. the Taihang and Yan Mountains, the Jing-Jin-Ji city cluster and Bohai Bay in the BTH region), can also induce local circulations that affect air pollutant concentrations (Liu et al., 2009; Wang et al., 2017). The distribution of air pollutants in Beijing and Tianjin is readily modified by mountain-valley ~~breezes~~ and sea-land breezes. Regional transport by local-~~scale~~ and weather-scale wind systems contribute significantly to the formation of severe haze events in the BTH region (Zheng et al., 2015; Sun et al., 2016; Ma et al., 2017; Jiang et al., 2015b). Dang et al. (2019) reported that regional transport was the most important process for the formation of severe winter haze days in the BTH region with a relative contribution of 65.3 %. Transport of aerosols to the BTH region by multi-scale circulations was also reported by Miao et al. (2017). However, due to a lack of dense vertical and horizontal spatial coverage of meteorological and aerosol observations, aerosol transport mechanisms and their effect on the explosive growth of ~~particular particlesmatter~~ in the BTH region are uncertain on both urban and smaller scales.

During a severe haze pollution event in 2015 in Beijing, a haze front (HF) ~~phenomenon~~ was reported on an internet social network, and also was intensively observed e.g. by scanning lidars and instrument networks during the 3-year field campaign of the Study of Urban Rainfall and Fog/Haze (SURF; Liang et al., 2018). This HF was identified by a sharp contrast in $PM_{2.5}$ concentration and a convergence line in the surface wind field. ~~The haze front~~It resulted in $PM_{2.5}$

concentration increases of more than 200 μg m^{-3} in a half hour or less when it passed over. This visible haze front in Beijing resembled the smog front noted by Ahrens (2003) but differed in that its formation mechanism ~~is~~ was foehn winds. The foehn is characterized by a decrease in cloudiness on the lee side of mountains and warm, dry, strong and gusty winds (Brinkmann 1971; Richner and Hächler 2013). The foehn warming mechanisms are summarized into four types (Elvidge and Renfrew 2016): isentropic drawdown, latent heating and precipitation, mechanical mixing due to turbulence, and radiative heating. Foehns occur downstream of most major mountain ridges in the world (Drechsel and Mayr 2008; Nkemdirim and Leggat 1978; Norte 2015; Takane and Kusaka 2011; Zhao et al., 1993). Beijing ~~city~~ is located on the plains adjacent to the southwest-northeast oriented Taihang Mountains and the northwest-southeast oriented Yan Mountains to the west and north, respectively. Due to this topography, Beijing is often affected by foehns especially in the plains areas adjacent to the mountains (Li et al., 2016, Wang et al., 2012a, 2012b). The temperature can increase sharply in a short time: for example, Luo et al. has reported an intense foehn warming event in which surface air temperature increased by more than 10℃ per hour in Beijing (Luo et al., 2020). Despite ~~the fact that the~~a long history of foehn ~~has been~~ investigations~~ed for a long time~~, there are few studies of the influence of foehns on air pollution, especially in the BTH region which has, for decades, been a worldwide hotspot for studying air pollution (Gohm et al. 2009; Li et al. 2015; McGowan et al. 1996, 2002). Also, very few studies have reported foehn-related fronts. Vergeiner (2004) reported a "minifront" or a convergence line between the up-valley flow and the down-valley foehn flow that was maintained ~~near the surface layer~~ in the Wipp Valley, Austria. Li et al. (2015) found that a ground-based foehn colliding with a thermally-driven valley breeze formed a "minifront" in Urumqi, China, indicating that the foehn can play a critical role in the formation of severe air pollution events in ~~this~~ that area. Nonetheless, foehn-related haze fronts seem to have never been investigated in the BTH region. Foehns usually come from western, northwestern and northern mountain areas in the Heibei-Beijing region, which are usually less polluted than the adjacent plains area in this region. Hence, foehns tend to increase visibility and decrease $PM_{2.5}$ concentrations in plains areas (Yang et al., 2018). In our case study, the foehn initially decreased $PM_{2.5}$ concentrations in the northern plains area of Beijing, and then interacted with a polluted air mass leading to severe pollution in the urban area. This latter dramatic consequence has not been reported in previous studies. The goal of our study ~~is~~ was to investigate the structure and formation of this foehn-related haze front on small scales in order to improve our understanding of the role of the foehn in air pollution events in the BTH region. Intensive measurements from SURF as well as routine measurements across the BTH region and historic data sets are described in Sect. 2. In Sect. 3, we examine the characteristics and evolution of the haze front. In Sect. 4, we compare the formation of a sea breeze front and a haze front, and discuss the main reason for HF propagation and the role of the foehn on air pollution. Sect. 5 is a summary.

2 Instrumentation, observations and data

Figure 1 and Table 1 shows the main observation sites mentioned here. The IAP site, which has been operated by the Institute of Atmospheric Physics (IAP) since 1978, has a 325 m high meteorological tower collocated with a ground-based Doppler lidar (Windcube 100S, Leosphere) and a mini-micropulse aerosol lidar (M~~m~~ini-MPL, SigmaSpace). The Doppler lidar profiled the mean wind using the Doppler beam swing (DBS) scan mode. The M~~m~~ini-MPL lidar profiled

aerosols and normalized relative backscatter (NRB). Wind direction and speed, air temperature, and relative humidity were measured at 15 levels (8, 15, 32, 47, 65, 80, 100, 120, 140, 160, 180, 200, 240, 280, 320 m) on the tower. Three-dimensional sonic anemometers, downward- and upward-pointing pyrgeometers and pyranometers (CNR1, Kipp & Zonen) and CO_2/H_2O concentration sensors (LI-7500) were installed at 47 m, 140 m and 280 m. The instrumentation at the IAP site is described in detail by Li et al. (2018b).

A M~~m~~ini-MPL lidar was installed at the top of the office building of the Institute of Urban Meteorology (IUM), executing a plan-position indicator (PPI) scan mode at a 5 ^{o} elevation angle and every 10 ^{o} of azimuth angle from 230 ^{o} to 340 ^{o} (Fig. 5d). Collocated with the Mini-MPL lidar, a portable automated weather station (AWS) measured wind speed and direction, air temperature, and relative humidity at the IUM building top, about 30 m above the ground level. In order to compare surface meteorological variables around the IUM site with other surface stations, meteorological data every 5 minutes from an AWS at the Chedougou (CDG) site, ~ 1 km north of the IUM site, was jointly analyzed with data from IUM. An air quality station on the ground ~ 40 m south of the IUM office building provided 5-minute mean $PM_{2.5}$ concentrations. A weather camera facing west was also installed in a room on the 9th floor of the office building taking photos every 30 s. ~~Due to the absence of a surface weather station at the IUM site, meteorological data every 5 minutes from an automated weather station (AWS) at the Chedougou (CDG) site, ~ 1 km north of the IUM site, was jointly analyzed with data at IUM.~~ An operational wind profiler was installed at the Haidian (HD) National Weather station site. We also used radio soundings launched twice daily at the Guanxiangtai (GXT) site. Hourly observations of $PM_{2.5}$ from all the air quality stations were obtained from the website of the Ministry of Ecology and Environmental of the People's Republic of China (http://106.37.208.233:20035). We used hourly $PM_{2.5}$ data at Aotizhongxin (AOT) site, ~3 km northeast of the IAP site, and Yizhuang (YZ) site, ~4 km northeast of the GXT site, to roughly represent $PM_{2.5}$ concentrations at IAP and GXT, respectively. At the Changping (CP) site, the AWS of the Beijing Meteorology Service (BMS) is very close to the air quality station of the Beijing Municipal Ecological Environment Bureau (BMEEB). During the study period, the Himawari satellite provided cloud images over the Beijing area every 10 minutes. ~~The p~~Pictures of this infrequent haze front were initially released by internet social communities, (e.g. SINA Weibo~~ -- (~~equivalent to Chinese Twitter). Based on time and location information, we selected two photos shown in Figure 1. All the observation heights used in this study are from ground level (AGL). Also, in order to investigate foehn occurrence frequency and its relationship to $PM_{2.5}$ concentrations in Beijing, 1 year of AWS data at CP, AOT and GXT, and $PM_{2.5}$ data at CP, AOT and YZ from 1 March 2015 to 29 February 2016 are used.

3 The evolution and characteristics of the haze front

3.1 Regional background of weather conditions and air pollution ~~and weather conditions~~

A 500 mb trough passed Beijing at 08:00 LST (local standard time; Beijing time) on 24 December (Fig. 3a). Meanwhile, the winds at 850 mb were predominantly northwesterly (Fig. 3c) which agreed well with the radiosonde (Fig. 2b) and wind profiler (Fig. 2c) observations. Winds were predominantly northeasterly or northerly at ~ 500 m AGL (Fig. 2d, Fig. 9c). On the surface, fog was reported in Hebei and Shandong Provinces, and easterly light winds were reported in Beijing by surface meteorological stations (Fig. 3e). At 20:00 LST, the 500 mb trough moved to eastern

China and the eastern part of the Korean peninsula (Fig. 3b). The upper air flow at 850 mb continued northwesterly (Fig. 3d). There was a weak surface high centered north of Beijing. The pressure gradient was weak with weak southwesterly surface flow in Beijing (Fig. 2c, Fig. 3f). The synoptic pattern at 20:00 LST, with a weak surface pressure gradient, southerly weak flows and no obvious synoptic weather system passage, is one situation that can typically exacerbate air pollution. According to Wang (2020), this circulation pattern accounts for 46% of all circulation types during winter in the BTH region.

This HF occurred on 24 December 2015 after a severe air pollution event. The mean $PM_{2.5}$ concentrations of CP, AOT and YZ varied between 300-400 μg m^{-3} on the morning ~~on~~ of 23 December, which is a severe Air Quality Index (AQI) pollution level (Fig. 2a). Thereafter, two significant $PM_{2.5}$ concentrations decreasing occurred at around noon and midnight on that day. During the day on 24 December, ~~Thereafter,~~ the mean –$PM_{2.5}$ concentration decreased to ~~~100~~ 73 μg m^{-3} at 0~~8~~7:00 LST~~ on 24 December~~. At 11:00 LST, the $PM_{2.5}$ concentration at YZ sharply increased 221 μg m^{-3} in one hour. At 13:00 LST, the $PM_{2.5}$ concentration of CP decreased from 112 μg m^{-3} to 32 μg m^{-3}. The $PM_{2.5}$ concentration at AOT stayed below 80 μg m^{-3} until 22:00 LST when its $PM_{2.5}$ concentration sharply increased 268 μg m^{-3} in one hour. The following day, the mean $PM_{2.5}$ concentration exceeded 500 μg m^{-3} at 14:00 LST. ~~and increased steadily up to 500 μg m^{-3} by afternoon of the next day. A 500 mb trough passed Beijing at 08:00 LST on 24 December (Fig. 3a). thepredominantly Winds were predominantly westerly or northwesterly at ~ 500 m AGL (Figure 2a, 2b, 2d). On the surface, a weak cold front was west of Beijing. On the right side of the cold front, fog was reported in Hebei and Shandong Provinces, and easterly lightflow was reported in Beijing by surface meteorological stations. At 20:00 LST, ncontinuedthere was a weak surface high centered north of Beijing. The pressure gradient was weak with weak southwesterly surface flow in Beijing (Fig. 2c, Fig. 3f).~~

3.2 The evolution ~~of the HF~~and characteristics of the HF and foehn winds

The visible channel true color images from the Himawari satellite clearly showed the movement and evolution of the HF~~ as well as a fog dense white fog coveringed northeastern Tianjin and half of Xianghe county of Heibei Province at 08:00 LST (Fig. 4a)~~. Normally, on the true color satellite images, clouds look white and gray and tend to have texture; haze is usually featureless and pale gray or a dingy white; fog looks similar to the color of clouds but without texture. However, clouds, fog and haze are sometimes difficult to distinguish from satellite imagery. Hence, we referred to weather phenomena, visibility and $PM_{2.5}$ concentration observed by surface meteorological and air quality stations to distinguish them. A dense fog covered northeastern Tianjin and half of Xianghe county of Heibei Province at 08:00 LST (Fig. 4a). Meanwhile, the Beijing area was clear with low pollution. Southwest-northeast oriented clouds partly shadowed the fog in Tianjin and Bohai Bay. ~~Left~~ West of the fog~~ front~~, the gray-white shading indicated hazy air with its front extending just into the boundary of Beijing (Fig. 4a). The edge of the hazy air mass corresponding to the HF line began to impact the GXT site (the blue dot, Fig. 4b, Fig. 11) at 10:00 LST followed by expanding fog areas. The HF line moved slowly to the northwest while the fog areas shrank quickly due to increasing solar radiation. A west-east oriented high cloud street overlapped the hazy and foggy areas (Fig 4d). After 16:00 LST, the fog disappeared and the HF line subsequently impacted the FS, CBD and IUM sites (Fig. 1, Fig. 5), leaving a smaller unpolluted urban area on the northwestern plains area in Beijing.

Based on the dense AWSs and air quality monitoring station coverage, the HF line was identified by sharp contrasts in $PM_{2.5}$ concentrations, temperature and humidity between the warm and cold air masses and the convergence line of the surface wind field (Fig. 6-7, Fig. S1-S3), which was also consistent with the front edge of the hazy air mass seen in the satellite images (Fig. 4). The foehn winds, with higher temperature and lower humidity, first occurred in the northwestern plain area and its adjacent mountain area with northerly winds at speeds of 6 m s^{-1} - 10 m s^{-1} from 11:00 to 12:00 LST (Fig. 6a). The foehn winds with the warm, dry, and clean air collided with more southerly or southeasterly winds with the cold, wet, and polluted air and resulted in oscillations of the HF line (Fig. 6-7). The HF line slowly advanced northwesterly with the southern part moving at about 2.5 km h^{-1} (Fig. 6; Fig S2). The $PM_{2.5}$ contrast between the clean and polluted air masses was more than 200 μg m^{-3} (Fig. 11). At 16:00 LST, the west-east oriented HF line crossed the main urban area and reached the IUM site (Fig. 6b, 7b). As the foehn began to decrease in intensity and retreat, and radiative heating decreased in late afternoon, the warm-dry air mass became weaker and shrank, leading to dissolution of the HF. After the northerly gusty winds decreased after sunset, the polluted air mass moved consistently toward the relative warm-dry and clean areas, resulting in severe pollution over most of the plains except for a small area on the northwestern plains adjacent to the mountains (Fig. S2-S3, Fig. S6-S7).

We used the CP, CDG and GXT sites (locations in Fig. 1) to investigate characteristics before and after the hazy air mass passed through. The northernmost site CP was mostly unaffected by the hazy air mass during 24 December. The southernmost site GXT was affected by the hazy air mass the earliest at 10:00 LST on 24 December. Afterward, the $PM_{2.5}$ concentration at GXT varied from 349 to 515 μg m^{-3} until midnight (Fig. 8e). The $PM_{2.5}$ concentration at CP was the lowest among three sites with a maximum of 148 μg m^{-3} at 11:00 LST and a minimum of 26 μg m^{-3} at 15:00 LST. The half-hourly temperature record showed that air temperature at CP increased significantly at 11:00 LST due to the foehn; in contrast, air temperature decreased significantly at CDG and GXT. Meanwhile, humidity decreased and wind speed increased at CP due to the foehn. The warm and dry foehn wind was initially detected over the northwestern mountains and plains of Changping County at around 11:00 LST, with a significant increase in temperature and the north wind component, and decrease in humidity. Wind profiler observations at HD also showed enhanced upper-air winds. From 10:00 to 13:00 LST, air temperature increased from 1.9℃ to 6℃, relative humidity decreased from 49% to 24%, and wind speed increased from 1 m s^{-1} to 4.6 m s^{-1} at CP. The foehn affected CDG at about 12:00 LST and IAP at 13:00 LST before colliding with a cold, wet, and hazy air mass. At 11:00 LST, an urban heat island (UHI) formed in the main urban areas mainly due to intense solar heating under a clear and clean sky but also from the heat released by urban activities. At 12:00 LST, the warm-dry air mass driven by the gusty foehn merged with the UHI, enlarging the coverage of the warm air mass. When the HF passed over CDG, the humidity and $PM_{2.5}$ concentrations significantly increased, the pressure slightly increased, but the temperature slightly decreased (Fig. 8). CDG was also affected by the foehn at around 12:00 LST, 1.5 hours later than CP, with accompanying temperature and wind speed increases, and decrease in humidity.

Aerosol lidar observations showed fine structures of the HF and its evolution. The ~~Min-MPL~~Mini-MPL at IUM scanned the HF passage using the PPI mode (Fig. 5c). The lidar initially detected a hazy air mass to the southwest far away from the lidar site. As the HF

approached, the outline of the polluted air mass was clearly visible against the sky and buildings on the weather camera photos (t1, Fig. 5e). When the HF arrived at the IUM site, the building view was blurred by the hazy air mass (t2, Fig. 5e). Surface wind direction changed suddenly from NNW to WSW. The $PM_{2.5}$ concentration jumped from ~10 to 269 μg m^{-3} in 10 minutes (Fig. 5b). The wind direction suddenly changed to northerly at 16:30 LST resulting in an abrupt $PM_{2.5}$ concentration decrease to 11 μg m^{-3} (Fig. 5b) and the visibility increased as evidenced by some visible buildings (t3, Fig. 5e). In less than 10 minutes, the wind direction reverted again from N to NNW resulting in a $PM_{2.5}$ concentration increase to 106 μg m^{-3} (Fig. 5b) and again blurred the building view at 16:39 LST (t4, Fig. 5e). The scans showed five pollution 'waves' successively ~~touched down at~~impacting the site and consequently led to severe pollution at 19:30 LST at IUM (Fig. 5b, 5c). The IAP site, 8 km northeast of IUM, was affected by the hazy air mass at around 20:30 LST according to vertically scanning lidar observations at this site (Fig. 5a).

~~Based on the dense AWSs and air quality monitoring station coverage, we were able to analyze surface distribution patterns of air temperature and humidity as they were affected by air flows and $PM_{2.5}$ concentrations in the plains areas. The HF line was identified by temperature and humidity contrasts between the warm and cold air masses and the convergence line of the surface wind field (Fig. 6-7, Fig. S1-S3), which was also consistent with the front edge of the hazy air mass seen in the satellite images (Fig. 4). The warm, dry, and clean air mass with more northerly winds was surrounded by~~collided with ~~the cold, wet, and polluted air mass with more southerly or southeasterly winds (Fig. 6-7)~~ and resulted in ~~oscillations of~~. T~~t~~he position of the HF line~~,~~ ~~oscillated due to the collision between the two air masses. The HF line slowly advanced northwesterly with the southern part moving at about 2.5 km h^{-1} (Fig. 6). The $PM_{2.5}$ contrast between the two air masses was more than 200 μg m^{-3}. At 16:00 LST, the west-east oriented HF line crossed the main urban area and reached the IUM site. Later that night, the wet and hazy air mass overlay most of the plains except for a small area on the northwestern plains adjacent to the mountains (e.g., the CP site). As the foehn began to decrease and retreat, and radiative heating decreased in late afternoon, the warm-dry air mass became weaker and shrank, leading to dissolution of the HF. After the northerly gusty winds decreased after sunset, the polluted air mass moved quickly toward the relative warm-dry and clean areas, resulting in severe pollution over most of the plains areas in Beijing.~~

~~3.3 Characteristics of the HF and foehn winds~~

~~We used the CP, CDG and GXT sites (locations in Fig. 1) to investigate characteristics before and after the hazy air mass passed through. The northernmost site CP was mostly unaffected by the hazy air mass during 24 December. The southernmost site GXT was affected by the hazy air mass the earliest at 10:00 LST on 24 December. Afterward, the $PM_{2.5}$ concentration at GXT varied from 349 to 515 μg m^{-3} until midnight (Fig. 8e). The $PM_{2.5}$ concentration at CP was the lowest among three sites with a maximum of 148 μg m^{-3} at 11:00 LST and a minimum of 26 μg m^{-3} at 15:00 LST. The three-hourly temperature tendency showed that air temperature at CP increased significantly at 11:00 LST due to the foehn; in contrast, air temperatures decreased significantly at CDG and GXT. Meanwhile, humidity decreased and wind speed increased at CP due to the foehn. The warm and dry foehn wind was initially detected over the northwestern mountains and plains of Changping County at around 11:00 LST, with a significant increase in temperature and the north wind component, and decrease in humidity. Wind profiler observations at HD also showed~~

~~enhanced upper-air winds. From 10:00 to 13:00 LST, air temperature increased from 1.9℃ to 6℃, relative humidity decreased from 49% to 24%, and wind speed increased from 1 m/s to 4.6 m/s at CP. The foehn affected CDG at about 12:00 LST and IAP at 13:00 LST before colliding with a cold, wet, and hazy air mass. At 11:00 LST, an urban heat island (UHI) formed in the main urban areas mainly due to intense solar heating under a clear and clean sky but also due to the heat released by urban activities. At 12:00 LST, the warm-dry air mass driven by gusty the foehn merged with the UHI, enlarging the coverage of the warm air mass. When the HF passed over CDG, the pressure significantly increased (~0.5 hpa, Fig. 8a) as well as humidity and $PM_{2.5}$ concentrations, but temperature slightly decreased (Fig. 8b). CDG was also affected by the foehn at around 12:00 LST, 1.5 hours later than CP, with accompanying temperature and wind speed increases, and decrease in humidity.~~

Using the doppler lidar and the 325-m tower concurrent observations at IAP, we analyzed the vertical structure of the foehn winds and the HF. At ~~IAP~~ around noon, the Doppler lidar detected a northwesterly wind and ~~an~~ a significant increased updraft ~~increased significantly~~ between 450 m and 1250 m height above the surface, and the wind direction below 500 m changed from northeast to northwest (Fig. 9). Concurrently, the tower temperatures also significantly increased and relative humidity decreased, and the wind profiles changed below 320 m (Fig. 10a-b), which implies that IAP was affected~~ing~~ by the foehn at this time. The temperature and ~~increased mainly from 12:00 LST to 19:00 LST when~~ turbulence ~~also~~ increased significantly mainly between 12:00 LST to 19:00 LST (Fig. 10c). As the HF approached, the wind weakened, the wind direction changed to the southwest, and the humidity increased sharply. The ~~atmosphere~~ boundary layer became more stably stratified near the surface, leading to enhanced pollution in the lowest ~~below a~~ few ~~the~~ hundred~~s~~ meter~~s level~~.

The solar radiation discrepancy between the clean and the polluted air mass was pronounced. Figure 11 shows downward shortwave radiation (DR) at IAP and GXT, and $PM_{2.5}$ concentrations at AOT and YZ. Aerosols reduced the DR to 225 W m^{-2} at GXT at 11:00 LST, 36 W m^{-2} less than IAP. The radiation difference between IAP and GXT was 174 W m^{-2} at 13:00 LST. Meanwhile, the $PM_{2.5}$ concentration was 456 μg m^{-3} greater at YZ than ~~ATZX~~AOT.~~—~~ At GXT, higher concentrations of aerosol particles in the polluted air mass scattered more solar radiation and reduced the amount of solar radiation at the ground, leading to weaker turbulence and lower PBL height which further enhanced the aerosol concentration near the ground. In contrast, at IAP~~,~~ there ~~were~~ was less aerosol ~~particulates~~, more radiation and stronger turbulence resulting in ~~higher~~ a deeper PBL ~~height~~ and less air pollution ~~ant concentration~~ near the ground.

4 Discussion

The formation of the HF is illustrated in Figure 12. The fundamental process of HF formation is similar to the concept of colliding density currents ~~illustrated~~ discussed by Simpson (1997) and Kingsmill et al. (2003), ~~i.e,~~due to the collision of a gust front with a sea-breeze front (SBF). This results in high concentrations of pollutants in the convergence zone of the front (Yoshikado et al., 1996; Dong et al., 2017; Li et al., 2019). As noted by Miller et al., (2003), who described the structure and characteristics of the SBF in detail, the sea breeze occurs under ~~relatively~~ mostly cloud-free skies, when the surface of the land heats up more rapidly than the sea. But in our case, the coastal area of Bohai Bay was covered mostly by clouds, fog, and haze during the daytime (Fig. 4), which decreased the contrast between the land and the sea and inhibited the sea breeze.

Also, sea breezes occur normally around 11:00 LST in the Bohai Bay area in winter, which is later than in summer (Qiu and Fan, 2013). The typical speed of a SBF is 3.4 m s^{-1} (Simpson et al., 1977), considerably larger than the observed HF speed of ~0.7 m s^{-1}. ~~Again~~Although, the front we studied was not a SBF~~,; nevertheless,~~ the SBF has some similarities in shape and formation to the HF in our study. The sea breeze is one example of a gravity or density current, which ~~are~~ is primarily a horizontal flow~~s~~ generated by a density difference of only a few percent. Field studies have confirmed that the SBF, as part of the sea breeze gravity current, has aspects of the sea breeze head (SBH), which had been simulated by Simpson (1994, 1997) using laboratory tanks and two bodies of water of slightly different densities. Likewise, in our case, a temperature difference between the warm ~~air mass~~ and ~~the~~ cold air mass resulted in a density difference between these air masses. Figures S4-S7 show air density distribution overlapping surface wind vectors and $PM_{2.5}$ concentrations. Note ~~in these figures~~ that the biggest gradient of air density corresponds to the wind convergence line as well as the HF line. Both the radiative heating difference between northern and southern areas, and the warm and dry foehn are key factors producing warm air masses. Southern hazy air masses reflect more solar radiation, and thus inhibit an increase in surface temperature and turbulence mixing, leading to colder and denser air. In contrast, solar radiative heating enhances heating of the northerly clear and cleaner air mass which concurrently was affected by the warm foehn, leading to warmer and less dense air. The lower density air mass collides with the higher density air mass and subsequently overrides the denser air mass (Fig. 1c; Fig. 5e; Fig. 12). This aspect is very similar to the SBF. The warmer air overriding the cold-wet air mass also intensifies the inversion at the top of the boundary between two air masses, limiting the growth rate of the underlying layer and increasing its pollutant concentration. The interface between the warm-dry air mass and the cold-wet air mass formed the HF and a significant convergence line at the surface. This kind of convergence line can sometimes be found during air pollution events when pollutants transferred by southerly winds encounter northerly mountain winds at night in the BTH region (Li et al, 2019; Liang et al., 2018).

Typically for clear daytime conditions, the horizontal temperature differences between the air over mountains and the adjacent plains can produce up-slope, up-valley, and plains-mountain winds, which are usually weak and often overpowered by strong foehns (Whiteman, 2000), and intensified wind speed in the upper air (Fig. 2d) as is the case here. Our results also show that the pressure difference between air masses is about 0.2~~5~~ hP~~p~~a before and after the HF passage (Fig. 8). This pressure gradient forcing creates a seesaw clash between the polluted and the clean air masses. The polluted air mass repeatedly encroaches into the clean air mass and is pushed back by the clean air mass. Eventually the polluted air mass wins. The lidar observed five wave-like polluted air invasions (Fig. 5). Thus the pressure difference between the air masses due to different air densities, although small, caused the hazy air mass to slowly swing north or northwest, and inflicted severe pollution on the urban area. Li et al., 2016 showed that the polluted aerosol concentration in southern Beijing is normally higher than in the urban and northern rural areas of Beijing (Li et al., 2016). For typical regional air pollution events in Beijing, air pollutants are mainly transported from surrounding areas, especially Hebei Province and Tianjin, south of Beijing (Zheng et al., 2015; Zheng et al., 2018). Both urban heat island effects and aerosol radiation forcing result in polluted areas that are colder with higher air density than less polluted areas, leading to a weak pressure gradient between more polluted and less polluted air masses. During the daytime, the pressure gradient forcing by air density is ~~overlapped~~ overwhelmed by the

forcing of plains-mountain winds, valley breezes and urban heat island circulations, enhancing ~~air pollutant~~pollution transport from southern to northern areas. At night, if mountain-plain~~s~~ winds and mountain breezes are weak, the pressure gradient forcing by air density can transport polluted air toward less polluted areas, which seems not to have been discussed previously. It implies that the weak pressure gradient could play an important role in ~~on air pollutants~~pollution transport during the weak mountain-plain wind system and mountain-valley breeze periods.

In order to investigate the occurrence frequency of the foehn in Beijing, we analyzed one year of AWS data ($PM_{2.5}$ data) at three sites CP (CP), AOT (AOT) and GXT (YZ), representing northern suburban, urban and southern suburban areas, respectively (Table 2). For daily data sampled hourly, if meteorological variables of the CP site at one hour meet the following criteria: (1) one-hour temperature increase is the highest among the three sites and greater than 1.5℃ and at least 1.0℃ higher than that at the GXT site, (2) one-hour relative humidity tendency is negative, and (3) hourly wind direction is greater than 270 ° or less than 90 °, we define this day as a foehn case day. These criteria ensure that the CP site adjacent to the mountains has the most significant warming among three sites with the foehn coming from the mountain and with a relative humidity decrease, i.e. a typical foehn case. Note in Table 2 that during the months from OCT to MAR when severe haze events are also frequent in Beijing, there is a higher foehn frequency than other months. There are 16 foehn cases, about 55% of all cases, connected to air pollution events. In 10 cases, $PM_{2.5}$ concentrations for all sites decreased 24 hrs after the foehn's occurrence ‘(Type A)’. In one~~1~~ case, $PM_{2.5}$ concentrations for all sites increased after the foehn's occurrence ‘(Type B)’. In 5 cases, including the case in this article, $PM_{2.5}$ concentrations for all sites initially decreased then increased 24 hrs after the foehn's occurrence ‘(Type C)’. The foehn's effects on air pollution can be direct or indirect~~:~~. The direct effect is that gusty foehns transport air pollutants resulting in increasing or decreasing ~~air~~ pollution concentration depending on whether the foehns are polluted or clean. The more complicated indirect effect is alteration of~~s~~ air mass properties and boundary layer structure by dry and warm foehn winds, which then influences air pollution. It is worth noting that type B cases in Table 2, accounting for 17% of total foehn cases, are likely due to the indirect effect leading to heavier air pollution, and ~~need to~~should be investigated further.

5 Summary and implications

This is the first study to our knowledge in which an HF related to the foehn in the BTH region has been analyzed. Based on observations collected during SURF-15, we studied an HF on 24 December 2015 in Beijing. This HF was formed by the collision between a cold-humid polluted air mass with higher density and a warm-dry clean air mass with lower density which was mainly due to the foehn. Initially, fog occupied the plains areas southeast of Beijing associated with a hazy air mass early in the morning. The hazy-foggy air mass developed and invaded Beijing around noon. The fog dissipated in the afternoon. The warm-dry downslope foehn began to impact the northern plains before noon and moved ~~to the~~ south, gradually affecting other plains sites until colliding with the cold-wet polluted air mass south and east of the urban areas, leading to a convergence line and the HF boundary at noon. As the HF passed by surface sites, $PM_{2.5}$ concentrations increased by more than 200 μg m^{-3} in 10 minutes. Following the HF, four surges of polluted air invaded the IUM site and consequently produced severe pollution. The HF boundary was clearly visible from satellite images and weather camera photos during the daytime. The formation of the HF is very similar to the SBF, although the front in our study cannot be explained

as an SBF due to weak radiation and temperature contrast between the land and sea, its earlier occurrence time and long distance inland. The sloped boundary of the HF tilts toward the polluted air mass as a result of the warm-dry clean air mass overriding the cold-wet polluted air mass. The HF slowly swings toward northern and northwestern clean areas. Our results show that as the foehn wind weakened and retreated, the weak pressure gradient between the warm-dry air mass and the cold-wet air mass was the main factor forcing the polluted air mass to slowly move north or northwest.

We segregate the effect of the foehn on air pollution into two types: a direct and an indirect effect. This foehn-induced HF event gives us a good opportunity to investigate both direct and indirect effects of the foehn on air pollution and haze events. Some studies have revealed the direct effect of the foehn on air pollution: stronger gusty foehns could diminish or even eliminate air pollutants. For the seldom-studied indirect effect of the foehn, ~~it could~~ enhanced differences in radiation and air density between clean and polluted air masses~~,~~ results~~ing~~ in a weak pressure gradient between air masses which allows the polluted air mass to invade the clean air mass. This mechanism could be more dominant especially when upslope winds, valley winds, and plains-mountain winds retreat after sunset in Beijing. Also, warm-dry foehns could affect urban heat island and atmosphere stratification in the boundary layer, and further affect air pollution.

Although air pollution events in BTH region have been studied from different aspects over decades, few studies have investigated the influence of the foehn on air pollution. Therefore, we recommend further studies on the formation mechanism of the foehn and its effects on air pollution in the BTH region.

Data availability. The $PM_{2.5}$ data is available on the website ~~of Ministry of Ecology and Environmental of the People's Republic of China (https://quotsoft.net/air/,http://106.37.208.233:20035)~~sources from the China Environmental Monitoring Station and the Beijing Environmental Protection Testing Center. Other data are available at http://www.ium.cn:8088/~~http://www.ium.cn/dataCenter/~~ which archives the SURF filed data collected from 2015 and 2016. All data used in this study can also be requested from the corresponding author (jli@ium.cn).

Author contributions. JL, MZ had the original idea, JL, ZS, YD, ZC, YW and QL performed the integrative data analysis, JL, ZS, and DL wrote the manuscript. All authors discussed the results and commented on the paper.

Competing interests. The authors declare that they have no conflict of interest.

Acknowledgments. The authors would like thank the anonymous reviewers for their helpful comments. This work was supported by the National Natural Science Foundation of China (41875123); the Ministry of Science and Technology of China (Grant No. 2016YFC0203302); Beijing Natural Science Foundation of China (8171002). The National Center for Atmospheric Research is sponsored by the U. S. National Science Foundation.
~~This material is based upon work supported by the National Center for Atmospheric Research, which is a major facility sponsored by the National Science Foundation under Cooperative Agreement No. 1852977~~.

471
472

References

Ahrens C. D.: Meteorology Today: An Introduction to Weather, Climate and the Environment. Thomson Learning, USA, 2003.

Brinkmann, W.: What is a foehn?, Weather, 26, 230–239, doi:10.1002/j.1477-8696.1971.tb04200.x., 1971.

Chen, J., Li, Z., Lv, M., Wang, Y., Wang, W., Zhang, Y., Wang, H., Yan, X., Sun, Y., and Cribb, M.: Aerosol hygroscopic growth, contributing factors, and impact on haze events in a severely polluted region in northern China, Atmos. Chem. Phys., 19, 1327–1342, https://doi.org/10.5194/acp-19-1327-2019, 2019.

Dang, R. and Liao, H.: Severe winter haze days in the Beijing–Tianjin–Hebei region from 1985 to 2017 and the roles of anthropogenic emissions and meteorology, Atmos. Chem. Phys., 19, 10801–10816, https://doi.org/10.5194/acp-19-10801-2019, 2019.

Dong G., Y. L., Hao T.: Analysis of meteorological characteristics of heavy haze process in Tianjin in autumn and winter and the role of sea breeze, Environmental Science & Technology, 40, 117-123, https://doi.org/10.3969/j.issn.1003-6504.2017.10.020, 2017 (in Chinese).

Drechsel S, Mayr J.: Objective forecasting of Foehn winds for a subgrid-scale Alpine Valley, Weather Forecast 23:205–218. https:// doi:10.1175/2007WAF021.1, 2008.

Elvidge, A. D., and Renfrew, I. A.: The Causes of Foehn Warming in the Lee of Mountains, Bulletin of the American Meteorological Society, 97, 455-466, https://doi.org/10.1175/bams-d-14-00194.1, 2016.

Gao, Y., Zhang, M., Liu, Z., Wang, L., Wang, P., Xia, X., Tao, M., and Zhu, L.: Modeling the feedback between aerosol and meteorological variables in the atmospheric boundary layer during a severe fog–haze event over the North China Plain, Atmos. Chem. Phys., 15, 4279–4295, https://doi.org/10.5194/acp-15-4279-2015, 2015.

Gohm, A., Harnisch, F., Vergeiner, J., Obleitner, F., Schnitzhofer, R., Hansel, A., Fix, A., Neiniger, B., Emeis, S., and Schafer, K.: Air pollution transport in an Alpine valley: Results from airborne and ground-based observations, Boundary-Layer Meteorol., 131, 441–463, https:// doi:10.1007/ s10546-009-9371-9, 2009.

Guo, H., Cheng, T., Gu, X., Wang, Y., Chen, H., Bao, F., Shi, S., Xu, B., Wang, W., Zuo, X., Zhang, X., and Meng, C.: Assessment of $PM_{2.5}$ concentrations and exposure throughout China using ground observations, Sci. Total Environ., 601–602, 1024–1030, https://doi.org/10.1016/j.scitotenv.2017.05.263, 2017.

Han, S., Hao, T., Zhang, Y., Liu, J., Li, P., Cai, Z., Zhang, M., Wang, Q., and Zhang, H.: Vertical observation and analysis on rapid formation and evolutionary mechanisms of a prolonged haze episode over Central-Eastern China, Sci. Total Environ., 616–617, 135–146, https://doi.org/10.1016/j.scitotenv.2017.10.278, 2018.

Han, T., Liu, X., Zhang, Y., Qu, Y., Zeng, L., Hu, M., and Zhu, T.: Role of secondary aerosols in haze formation in summer in the Megacity Beijing, J. Environ. Sci., 31, 51–60, https://doi.org/10.1016/j.jes.2014.08.026, 2015.

Han, X., Zhang, M., Gao, J., Wang, S., and Chai, F.: Modeling analysis of the seasonal characteristics of haze formation in Beijing, Atmos. Chem. Phys., 14, 10231–10248, https://doi.org/10.5194/acp-14-10231-2014, 2014.

Huang, R. J., Zhang, Y., Bozzetti, C., Ho, K. F., Cao, J. J., Han, Y., Daellenbach, K. R., Slowik, J. G., Platt, S. M., Canonaco, F., Zotter, P., Wolf, R., Pieber, S. M., Bruns, E. A., Crippa, M., Ciarelli, G., Piazzalunga, A., Schwikowski, M., Abbaszade, G., Schnelle-Kreis, J., Zimmermann, R., An, Z., Szidat, S., Baltensperger, U., El Haddad, I., and Prevot, A. S.: High secondary aerosol contribution to particulate pollution during haze events in China, Nature, 514, 218–222, https://doi.org/10.1038/nature13774, 2014.

Huang, X., Wang, Z., and Ding, A.: Impact of Aerosol-PBL Interaction on Haze Pollution: Multiyear Observational Evidences in North China, Geophys. Res. Lett., 45, 8596–8603, https://doi.org/10.1029/2018gl079239, 2018.

Jiang, J. K., Zhou, W., Cheng, Z., Wang, S. X., He, K. B., and Hao, J. M.: Particulate Matter Distributions in China during a Winter Period with Frequent Pollution Episodes (January 2013), Aerosol Air Qual. Res., 15,

494–503, https://doi.org/10.4209/aaqr.2014.04.0070, 2015a.

Jiang, C., Wang, H., Zhao, T., Li, T., and Che, H.: Modeling study of $PM_{2.5}$ pollutant transport across cities in China's Jing–Jin–Ji region during a severe haze episode in December 2013, Atmos. Chem. Phys., 15, 5803–5814, https://doi.org/10.5194/acp-15-5803-2015, 2015b.

Kingsmill, D. E. and Crook N. A.: An observational study of atmospheric bore formation from colliding density currents, Monthly Weather Review, 131, 2985-3002, https://doi:10.1175/1520-0493(2003)131<2985:Aosoab>2.0.Co;2.,2003.

Li, K., Liao, H., Cai, W., and Yang, Y.: Attribution of Anthropogenic Influence on Atmospheric Patterns Conducive to Recent Most Severe Haze Over Eastern China, Geophys. Res. Lett., 45, 2072–2081, https://doi.org/10.1002/2017gl076570, 2018a.

Li, J., Sun, J., Zhou, M., Cheng, Z., Li, Q., Cao, X., Zhang, J.: Observational analyses of dramatic developments of a severe air pollution event in the Beijing area, Atmos. Chem. Phys., 18 (6), 3919-3935, https://doi.org/10.5194/acp-2017-909,2018b.

Li Q., L. J., Zheng Z., Wang Y., Yu M.: Influence of Mountain Valley Breeze and Sea Land Breeze in Winter on Distribution of Air Pollutants in Beijing-Tianjin-Hebei Region, Environmental Science, 40, 513-524, https://doi.org/10.13227/j.hjkx.201803193, 2019 (in Chinese).

Li, J., Du, H., Wang, Z., Sun, Y., Yang, W., Li, J., Tang, X., and Fu, P.: Rapid formation of a severe regional winter haze episode over a mega-city cluster on the North China Plain, Environ. Pollut., 223, 605–615, https://doi.org/10.1016/j.envpol.2017.01.063, 2017.

Li, L.,Wang, Z., Zhang, D. Chen, T., Jiang, L., and Li, Y.: Analysis of heavy air pollution episodes in Beijing during 2013–2014, Chinese Environmental Science, 36, 27–35, 2016 (in Chinese).

Li, X., Xia, X., Wang, L., Cai, R., Zhao, L., Feng, Z., Ren, Q., Zhao, K.: The role of foehn in the formation of heavy air pollution events in Urumqi, China. J. Geophys. Res. Atmos., 120, 5371–5384, https://doi.org/10.1002/2014jd022778, 2015.

Liang, X., Miao, S., Li, J., Bornstein, R., Zhang, X., Gao, Y., Cao, X., Chen, F., Cheng, Z., Clements, C., Debberdt, W., Ding, A., Ding, D., Dou, J. J., Dou, J. X., Dou, Y., Grimoond, C. S. B., Gonzalez-Cruz, J., He, J., Huang, M., Huang, X., Ju, S., Li, Q., Niyogi, D., Quan, J., Sun, J., Sun, J. Z., Yu, M., Zhang, J., Zhang, Y., Zhao, X., Zheng, Z., and Zhou, M: SURF: Understanding and predicting urban convection and haze, Bulletin of the American Meteorological Society, 99(7): 1391-1413, https://doi.org/10.1175/bams-d-16-0178.1, 2018.

Liu, Q., Jia, X., Quan, J., Li, J., Li, X., Wu, Y., Chen, D., Wang, Z., and Liu, Y.: New positive feedback mechanism between boundary layer meteorology and secondary aerosol formation during severe haze events, Sci. Rep., 8, 6095, https://doi.org/10.1038/s41598-018-24366-3, 2018.

Liu, S., Liu, Z., Li, J., Wang, Y., Ma, Y., Sheng, L., Liu, H., Liang, F., Xin, G., and Wang, J.: Numerical simulation for the coupling effect of local atmospheric circulations over the area of Beijing, Tianjin and Hebei province, Sci. China Ser. D, 52, 382–392, https://doi.org/10.1007/s11430-009-0030-2, 2009.

Liu, T., Gong, S., He, J., Yu, M., Wang, Q., Li, H., Liu, W., Zhang, J., Li, L., Wang, X., Li, S., Lu, Y., Du, H., Wang, Y., Zhou, C., Liu, H., and Zhao, Q.: Attributions of meteorological and emission factors to the 2015 winter severe haze pollution episodes in China's Jing-Jin-Ji area, Atmos. Chem. Phys., 17, 2971–2980, https://doi.org/10.5194/acp-17-2971-2017, 2017.

Liu, X. G., Li, J., Qu, Y., Han, T., Hou, L., Gu, J., Chen, C., Yang, Y., Liu, X., Yang, T., Zhang, Y., Tian, H., and Hu, M.: Formation and evolution mechanism of regional haze: a case study in the megacity Beijing, China, Atmos. Chem. Phys., 13, 4501–4514, https://doi.org/10.5194/acp-13-4501-2013, 2013.

Luo R., Zheng Y G., Chen M.: Mechanism of a rare night sudden intense warming event in Beijing and surrounding area. Meteorological Monthly, 46, 478-489, 2020 (in Chinese).

Ma, Q., Wu, Y., Zhang, D., Wang, X., Xia, Y., Liu, X., Tian, P., Han, Z., Xia, X., Wang, Y., and Zhang, R.: Roles of regional transport and heterogeneous reactions in the $PM_{2.5}$ increase during winter haze episodes in Beijing, Sci. Total Environ., 599–600, 246–253,https://doi.org/10.1016/j.scitotenv.2017.04.193, 2017.

McGowan, H. A., A. P. Sturman, M. Kossmann, and P. Zawar-Reza : Observation of foehn onset in the Southern Alps, New Zealand, Meteorol. Atmos. Phys., 79, 215–230, https://doi:10.1007/s007030200004, 2002.

McGowan, H. A., P. A. Sturman, and F. L. Owens : Aeolian dust transport and deposition by foehn winds in an alpine environment, Lake Tekapo, New Zealand, Geomorphology, 15(2), 135–146, https://doi:10.1016/0169-555X(95)00123-M, 1996.

Miao, Y., J. Guo, S. Liu, H. Liu, G. Zhang, Y. Yan, and J. He: Relay transport of aerosols to Beijing-Tianjin-Hebei region by multi-scale atmospheric circulations. Atmospheric Environment, 165, 35-45, https://doi.org/10.1016/j.atmosenv.2017.06.032, 2017.

Miller, S. T. K., Keim B. D., Talbot R. W., and Mao H.: Sea breeze: Structure, forecasting, and impacts. Reviews of Geophysics, 41(3), 1-31, https://doi.org/10.1029/2003rg000124, 2003.

Nkemdirim LC., Leggat K.: The effect of Chinook weather on urban heat islands and air pollution. Water Air Soil Pollut 9:53–67, 1978.

Norte, F.: Understanding and Forecasting Zonda Wind (Andean Foehn) in Argentina: A Review. Atmospheric and Climate Sciences, 5, 163-193. https://doi: 10.4236/acs.2015.53012, 2015.

Petäjä, T., Järvi, L., Kerminen, V.-M., Ding, A.J., Sun, J.N., Nie, W., Kujansuu, J., Virkkula, A., Yang, X., Fu, C.B., Zilitinkevich, S., Kulmala, M.: Enhanced air pollution via aerosol-boundary layer feedback in China. Sci. Rep. 6, 18998, https://doi.org/10.1038/srep18998, 2016.

Qiu X., Fang. S.: Progress of Sea-Land Breeze Study and Characteristics of Sea-Land Breeze in Three Coastal Areas in China, Meteorological Monthly, 39, 186-193, https://doi.org/10.7519/j.issn.1000-0526.2013.02.007, 2013 (in Chinese).

Ren, Y., Zhang, H., Wei, W., Wu, B., Cai, X., and Song, Y.: Effects of turbulence structure and urbanization on the heavy haze pollution process, Atmos. Chem. Phys., 19, 1041–1057, https://doi.org/10.5194/acp-19-1041-2019, 2019.

Richner, H. and Hächler, P.: Understanding and forecasting Alpine foehn, in Mountain Weather Research and Forecasting, Springer Atmospheric Sciences, edited by F. K. Chow, S. F. J. De Walker, and B. J. Snyder, pp. 219–260, Springer, Netherlands, 2013.

Simpson, J. E., D. A. Mansfield, and J. R. Milford, Inland penetration of sea-breeze fronts, Q. J. R. Meteorol. Soc., 103,47–76, 1977.

Simpson, J. E., Gravity Currents in the Environment and the Laboratory, 244 pp., Cambridge Univ. Press, New York, 1997.

Simpson, J. E., Sea Breeze and Local Wind, 234 pp., Cambridge Univ. Press, New York, 1994.

Steiner, A. L., Mermelstein, D., Cheng, S. J., Twine, T. E., and Oliphant, A.: Observed Impact of Atmospheric Aerosols on the Surface Energy Budget, Earth Interact., 17, 1–22, https://doi.org/10.1175/2013ei000523.1, 2013.

Su, T., Li, Z., and Kahn, R.: Relationships between the planetary boundary layer height and surface pollutants derived from lidar observations over China: regional pattern and influencing factors, Atmos. Chem. Phys., 18, 15921–15935, https://doi.org/10.5194/acp-18-15921-2018, 2018.

Sun, F., Zhang, D., Sun, R., Dong, X., Wang, X., Wang, Z., and Cheng, N.: Typical heavy pollution episode analysis on $PM_{2.5}$ in winter of Beijing, Environment Monitoring in China, 30, 1–12, https://doi.org/10.3969/j.issn.1002-6002.2014.06.001, 2014 (in Chinese).

Sun, Y. L., Jiang, Q., Wang, Z. F., Fu, P. Q., Li, J., Yang, T., and Yin, Y.: Investigation of the sources and

evolution processes of severe haze pollution in Beijing in January 2013, J. Geophys. Res.-Atmos., 119, 4380–4398, https://doi.org/10.1002/2014jd021641, 2014.

Sun, Y., Chen, C., Zhang, Y., Xu, W., Zhou, L., Cheng, X., Zheng, H., Ji, D., Li, J., Tang, X., Fu, P., and Wang, Z.: Rapid formation and evolution of an extreme haze episode in Northern China during winter 2015, Sci. Rep., 6, 27151, https://doi.org/10.1038/srep27151, 2016.

Takane, Y. and Kusaka H.: Formation Mechanisms of the Extreme High Surface Air Temperature of 40.9℃ Observed in the Tokyo Metropolitan Area: Considerations of Dynamic Foehn and Foehnlike Wind. J. Appl. Meteor. Climatol., 50, 1827–1841, https://doi.org/10.1175/JAMC-D-10-05032.1, 2011.

Tie, X., Huang, R.-J., Cao, J., Zhang, Q., Cheng, Y., Su, H., Chang, D., Pöschl, U., Hoffmann, T., Dusek, U., Li, G., Worsnop, D. R., and O'Dowd, C. D.: Severe Pollution in China Amplified by Atmospheric Moisture, Sci. Rep.-UK, 7, 15760, https://doi.org/10.1038/s41598-017-15909-1, 2017.

Vergeiner, J. : South foehn studies and a new foehn classification scheme in theWipp and Inn Valley, PhD thesis, Univ. of Innsbruck, Austria, 2004.

Wang X, Zhang R: Effects of atmospheric circulations on the interannual variation in PM2.5 concentrations over the Beijing–Tianjin–Hebei region in 2013–2018. Atmos Chem Phys 2020, 20(13):7667-7682.

Wang, Z., Ding, Y., Zhang, Y., Wang, C., Li J., Gu, Y.: Feature and Mechanism of the Foehn Weather on East Slope Taihang Mountains Ⅰ:Statistic Feature. PLATEAU METEOROLOGY, 31, 547-554, 2012a (in Chinese).

Wang, Z., Ding, Y., Zhang, Y., Fan, J., Zhang, S., Tian L.,: Feature and Mechanism of the Foehn Weather on East Slope Taihang Mountains Ⅱ:Case Analysis of the Effects of Lee Wave on Foehn Occurring and Moving, 31, 555-561, 2012b (in Chinese).

Wang, Y. H., Liu, Z. R., Zhang, J. K., Hu, B., Ji, D. S., Yu, Y. C., and Wang, Y. S.: Aerosol physicochemical properties and implications for visibility during an intense haze episode during winter in Beijing, Atmos. Chem. Phys., 15, 3205–3215, https://doi.org/10.5194/acp-15-3205-2015, 2015.

Wang, Y., Bao, S., Wang, S., Hu, Y., Shi, X., Wang, J., Zhao, B., Jiang, J., Zheng, M., Wu, M., Ruseel, A., Wang, Y., and Hao, J.: Local and regional contributions to fine particulate matter in Beijing during heavy haze episodes, Sci. Total Environ., 580, 283–296, https://doi.org/10.1016/j.scitotenv.2016.12.127, 2017.

Wang, Y., Yao, L., Wang, L., Liu, Z., Ji, D., Tang, G., Zhang, J., Sun, Y., Hu, B., and Xin, J.: Mechanism for the formation of the January 2013 heavy haze pollution episode over central and eastern China, Science China Earth Sciences, 57, 14–25, https://doi.org/10.1007/s11430-013-4773-4, 2013.

Whiteman, C. D.: Mountain Meteorology: Fundamentals and Applications, Oxford Univ. Press, New York, 2000.

Wu, J., Bei, N., Hu, B., Liu, S., Zhou, M., Wang, Q., Li, X., Liu, L., Feng, T., Liu, Z., Wang, Y., Cao, J., Tie, X., Wang, J., Molina, L. T., and Li, G.: Is water vapor a key player of the wintertime haze in North China Plain?, Atmos. Chem. Phys., 19, 8721–8739, https://doi.org/10.5194/acp-19-8721-2019, 2019.

Yang Xiaoliang, Y. M., Li Jiangbo, Zhang Shan: Impact Analysis of a Taihang Mountain Fohn on Haze Intensity. Meteorological Monthly, 44, 313-319, https://doi.org/10.7519/j.issn.1000-0526.2018.02.011, 2018.

Yoshikado Hiroshi and Tsuchida Makoto: High levels of winter air pollution uder the influence of the urban heat island along the shore of Tokyo Bay, Journal of Applied Meteorology, 35, 1804-1813, 1996.

Zhang, B., Wang, Y., and Hao, J.: Simulating aerosol–radiation–cloud feedbacks on meteorology and air quality over eastern China under severe haze conditions in winter, Atmos. Chem. Phys., 15, 2387–2404, https://doi.org/10.5194/acp-15-2387-2015, 2015.

Zhang, R. H., Li, Q., and Zhang, R. N.: Meteorological conditions for the persistent severe fog and haze event over eastern China in January 2013, Sci. China Earth Sci., 57, 26–35, https://doi.org/10.1007/s11430-013-4774-3, 2014.

Zhao, S., W. R., Guo Yanbo, Tan Jianlong, Shi Zhizeng: The Foehn in the Middle Range of Taihang Mountain. Meteorological Monthly, 19, 3-6, https://doi.org/10.7519/j.issn.1000-0526.1993.2.001, 1993 (in Chinese).

Zhao, X. J., Zhao, P. S., Xu, J., Meng,, W., Pu, W. W., Dong, F. He, D., and Shi, Q. F.: Analysis of a winter regional haze event and its formation mechanism in the North China Plain, Atmos. Chem. Phys., 13, 5685–5696, https://doi.org/10.5194/acp-13-5685-2013, 2013.

Zheng, G. J., Duan, F. K., Su, H., Ma, Y. L., Cheng, Y., Zheng, B., Zhang, Q., Huang, T., Kimoto, T., Chang, D., Pöschl, U., Cheng, Y. F., and He, K. B.: Exploring the severe winter haze in Beijing: the impact of synoptic weather, regional transport and heterogeneous reactions, Atmos. Chem. Phys., 15, 2969–2983, https://doi.org/10.5194/acp-15-2969-2015, 2015.

Zhong, J., Zhang, X., Wang, Y., Sun, J., Zhang, Y., Wang, J., Tan, K., Shen, X., Che, H., Zhang, L., Zhang, Z., Qi, X., Zhao, H., Ren, S., and Li, Y.: Relative contributions of boundary layer meteorological factors to the explosive growth of PM2:5 during the red-alert heavy pollution episodes in Beijing in December 2016, J. Meteorol. Res.-PRC, 31, 809–819, https://doi.org/10.1007/s13351-017-7088-0, 2017.

Zheng, Z., Xu, G., Yang, Y., Wang, Y., Li, Q.: Statistical characteristics and the urban spillover effect of haze pollution in the circum-Beijing region, Atmos. Pollut. Res. 9, 1062–1071, https://doi.org/10.1016/j.apr.2018.04.004, 2018.

Table 1. Latitude, longitude, altitude, site type and instrumentation at the main sites in Fig.1.

Site name	Latitude	Longitude	Altitude (m MSL)	Site type	Instrumentation
GXT	39.806	116.469	31	Meteorology	radiosonde, radiometer, wind profiler, AWS, pyranometer
IAP	39.974	116.371	29	Meteorology	325-m tower, sonic anemometers, doppler lidar, vertical scanning MPL, pyrgeometer and pyranometer
IUM	39.95	116.28	37	Meteorology & Air quality	PPI scanning MPL, weather camera, particulates sampler and analyzer
CDG	39.945	116.291	58	Meteorology	AWS
CP	40.223	116.212	76	Meteorology & Air quality	AWS, particulates sampler and analyzer
HD	39.987	116.291	46	Meteorology	AWS, wind profiler
AOT	39.982	116.397	–48	Meteorology & Air quality	AWS, particulates sampler and analyzer
YZ	39.795	116.506	–31	Air quality	particulates sampler and analyzer

※ AWS: automated weather station; MPL: micro pulse lidar; PPI: plain position indicator

672 **Table 2.** Number of foehn cases in Beijing from 1 March 2015 to 29 February 2016

		JAN	FEB	MAR	APR	MAY	JUN	JUL	AUG	SEP	OCT	NOV	DEC	Total cases
Clean cases		4	2	1	0	1	1	0	1	0	2	1	0	13
Polluted cases	Type A	1	2	2	0	1	0	0	0	0	2	0	2	10
	Type B	1	0	1	0	0	0	0	0	0	0	1	2	5
	Type C	0	0	0	0	0	0	0	0	1	0	0	0	1
All cases		6	4	4	0	2	1	0	1	1	4	2	4	29

673 Clean cases: foehn cases in which average $PM_{2.5}$ concentrations for CP, AOT and YZ is less than 50 μg m^{-3}.

674 Polluted cases: foehn cases in average $PM_{2.5}$ concentrations for CP, AOT and YZ is greater than 50 μg m^{-3}.

675 Type A: polluted cases where ~~with~~ $PM_{2.5}$ concentrations for CP, AOT and YZ sites ~~had~~ decreas~~ed~~ing within 24 hours from the
676 onset of foehn winds ~~since foehn's occurrence in 24 hours~~.

677 Type B: ~~polluted cases with $PM_{2.5}$ concentrations for CP, AOT and YZ sites initially decreasing then increasing since foehn's~~
678 ~~occurrence in 24 hours.~~polluted cases where $PM_{2.5}$ concentrations for CP, AOT and YZ sites initially decreased then increased
679 within 24 hours from the onset of foehn winds.

680 Type C: polluted cases ~~but~~ where $PM_{2.5}$ concentrations for CP, AOT and YZ sites ~~had~~ increas~~ing~~ed within 24 hours from the
681 onset of foehn winds.~~since foehn's occurrence in 24 hours~~.

682 All cases: all of clean cases and polluted cases.

683
684
685
686
687

Figure Captions

Figure 1. (a) Locations of observational stations (larger symbols with site name: main stations used here) along with the fourth, fifth and sixth ring roads (gray lines) in Beijing, China. Anonymous photos from SINA Weibo (like Twitter but in Chinese) at (b) Financial Street (FS) at 15:30 and (c) Central Business District (CBD) at 16:00 on 24 December 2015. Locations for taking the photos are shown as yellow stars in the upper map.

~~Figure 1. (a) Locations of main observational stations (red dots: meteorological stations; blue dots: air quality monitoring stations) used here, along with the fourth, fifth and sixth ring roads (blue lines) in Beijing, China. Anonymous photos from SINA Weibo (like Twitter but in Chinese) at (b) Financial Street (FS) at 15:30 and (c) Central Business District (CBD) at 16:00 on 24 December 2015. Locations for taking the photos are shown as yellow stars in the upper map.~~

Figure 2. (a) Hourly-mean $PM_{2.5}$ concentration of CP, AOT, YZ and 3-stations mean~~35 air quality stations~~ in Beijing from 23 ~~December~~ to 25 December. Temperature (solid), dew point (dashed), and wind vectors (in knots) from the radiosonde~~ sounding~~ profiles at (b) 00:00 UTC and (c) 12:00 UTC at GXT. (d) ~~The temporal variation of h~~Hourly wind-vector profiles from the wind profiler at HD on 24 December 2015.

Figure 3. The 500 mb weather maps at (a) 08:00 LST and (b) 20:00 LST, the 800 mb weather maps at (c) 08:00 LST and (d) 20:00 LST, and surface maps at (e) 08:00 LST and (f) 20:00 LST on 24 December 2015. The administrative boundaries of Beijing are marked in brown.

Figure 4. Cloud images from the visible channels of the Himawari satellite at (a) 08:00 LST, (b) 10:00 LST, (c) 12:00 LST, (d) 14:00 LST, (e) 15:00 LST, and (f) 16:00 LST on 24 December 2015. Red, yellow and blue dots are the locations of IUM, IAP and GXT, respectively. The purple lines indicate the location of the haze front.

Figure 5. (a) ~~The Min-MPL~~ Vvertical~~ly scanned~~ normalized relative backscatter (NRB) from the Mini-MPL at IAP. (b) 5-min average wind speed (red line), wind direction (triangles) ~~at CDG station~~ and $PM_{2.5}$ concentrations (blue line) at IUM. (c) The NRB from a ~~Min-MPL~~Mini-MPL at ~~IAP~~ IUM scanning in (d) plan position indicator (PPI) mode using 10^{o} horizontal angle intervals from 340^{o} to 220^{o} and at 5^{o} elevation angle. (e) Four photos taken by the weather camera at IUM at times t1, t2, t3 and t4 which are marked as red lines in the upper plot.

Figure 6. Temperature (colored ~~filled~~ dots coded according to the bottom color bar), wind vectors (2 m s^{-1} is one full bar) and $PM_{2.5}$ concentrations (purple circles; the size of the circle represents concentration values) in the plains area within and around Beijing at (a) 12:00 LST and (b) 16:00 LST. The blue lines indicate the ~~location of the~~ haze front location.

Figure 7. Same as Fig 6, but with relative humidity.

Figure 8. Half ~~Three h~~hourly (a) pressure anomaly~~tendency~~, (b) air temperature ~~tendency~~, ~~and~~ (c) specific humidity, and (d) wind speed (lines) and wind directions (colored dots), and (e) hourly $PM_{2.5}$ concentration at CP (red line), CDG (blue dash line) and GXT (black dash line) on 24 December 2015. The gray line indicates the time of HF passage at CDG.

Figure 9. Doppler lidar observations of (a) vertical wind velocity, (b) horizontal wind speed, (c) wind direction, and (d) carrier-noise-ratio (CNR) at IAP on 24 December 2015. The

gray line indicates the time of HF passage at IAP.

Figure 10. Temporal variations of (a) temperature (colored contours) and wind vectors, (b) relative humidity (colored contours) and wind vectors at 15 levels on the IAP tower, and (c) vertical velocity ~~variance~~ standard deviation at 47 m and 280 m on the IAP tower on 24 December 2015. The gray line indicates the time of HF passage at IAP.

Figure 11. The temporal variations of $PM_{2.5}$ concentrations at ~~ATZX~~AOT (blue bars) and YZ (red bars), and downward short-wave radiation at GXT and at heights of 47 m, 140 m and 280 m ~~at~~ on the IAP tower during daytime on 24 December 2015.

Figure 12. Schematic diagram of the haze front formation.

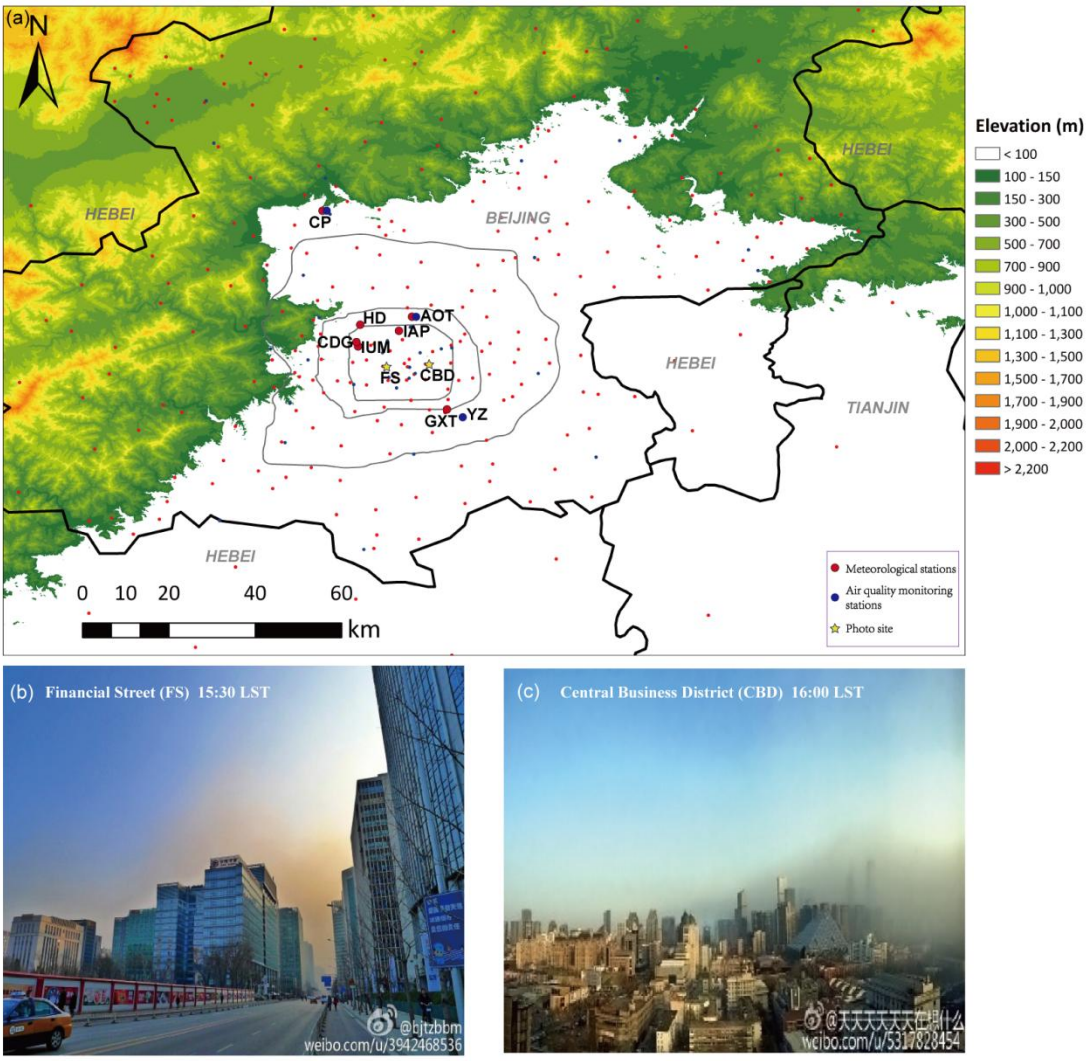

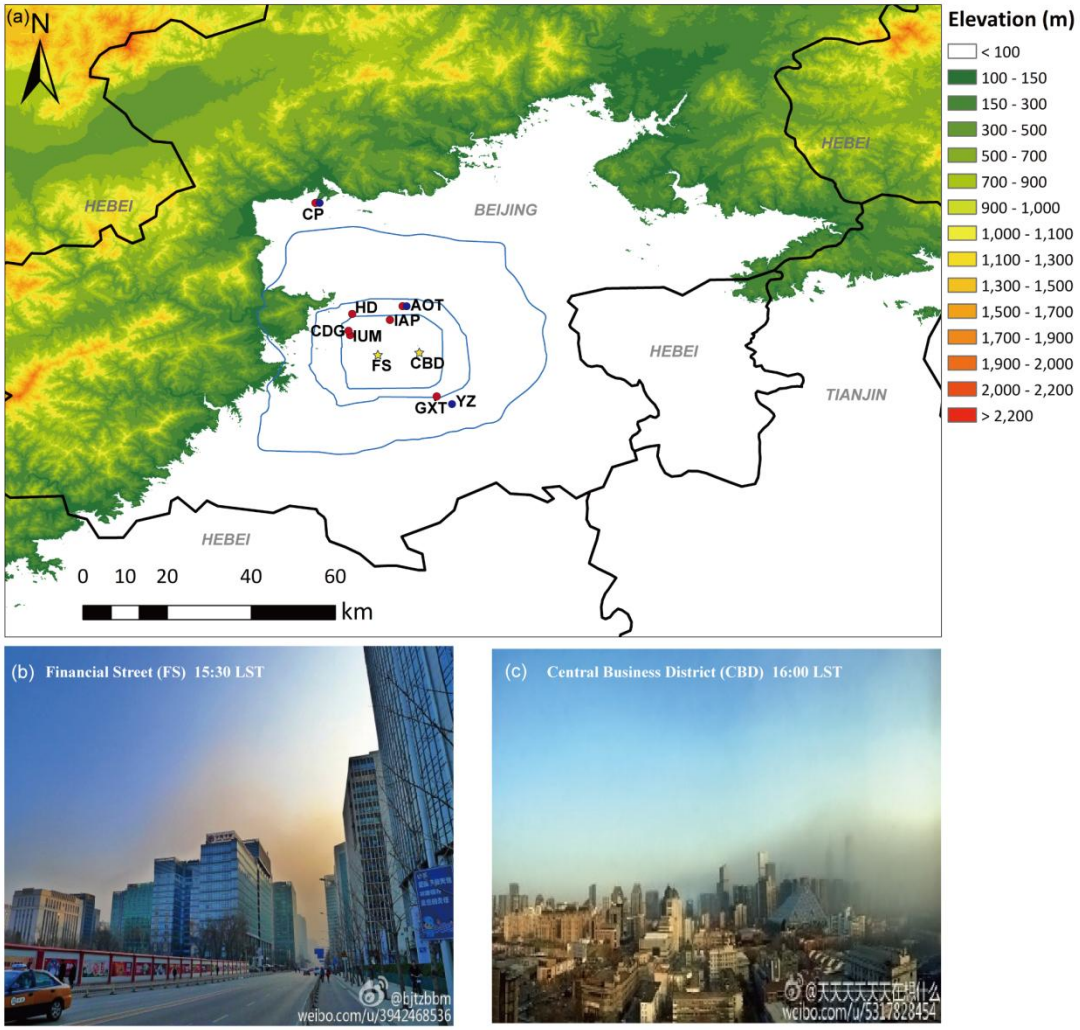

Figure 1. (a) Locations of ~~main~~ observational stations (larger symbols with site name: main stations used here~~red dots: meteorological stations; blue dots: air quality monitoring stations~~) ~~used here,~~ along with the fourth, fifth and sixth ring roads (~~blue~~ gray lines) in Beijing, China. Anonymous photos from SINA Weibo (like Twitter but in Chinese) at (b) Financial Street (FS) at 15:30 and (c) Central Business District (CBD) at 16:00 on 24 December 2015. Locations for taking the photos are shown as yellow stars in the upper map.

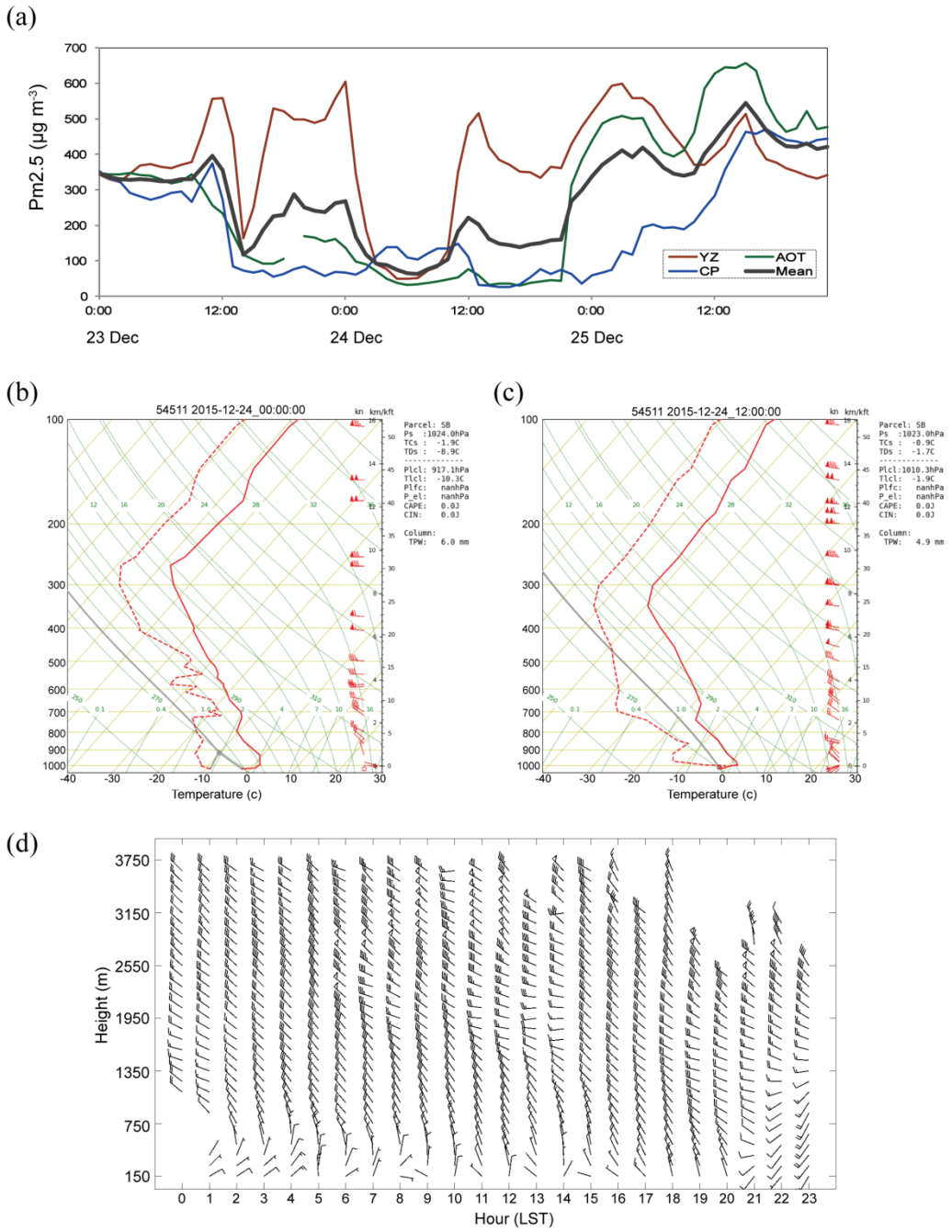
(a)
Pm2.5 (μg m-3)
700
600
500
400
300
200
100
0
0:00
12:00
0:00
12:00
0:00
12:00
23 Dec
24 Dec
25 Dec
YZ
AOT
CP
Mean
(b)
54511 2015-12-24_00:00:00
Parcel: SB
Ps :1024.0hPa
TCs : -1.9C
TDs : -8.9C
Plcl: 917.1hPa
Tlcl: -10.3C
Plfc: nanhPa
P_el: nanhPa
CAPE: 0.0J
CIN: 0.0J
Column:
TPW: 6.0 mm
Temperature (c)
(c)
54511 2015-12-24_12:00:00
Parcel: SB
Ps :1023.0hPa
TCs : -0.9C
TDs : -1.7C
Plcl:1010.3hPa
Tlcl: -1.9C
Plfc: nanhPa
P_el: nanhPa
CAPE: 0.0J
CIN: 0.0J
Column:
TPW: 4.9 mm
Temperature (c)
(d)
Height (m)
3750
3150
2550
1950
1350
750
150
0 1 2 3 4 5 6 7 8 9 10 11 12 13 14 15 16 17 18 19 20 21 22 23
Hour (LST)

753

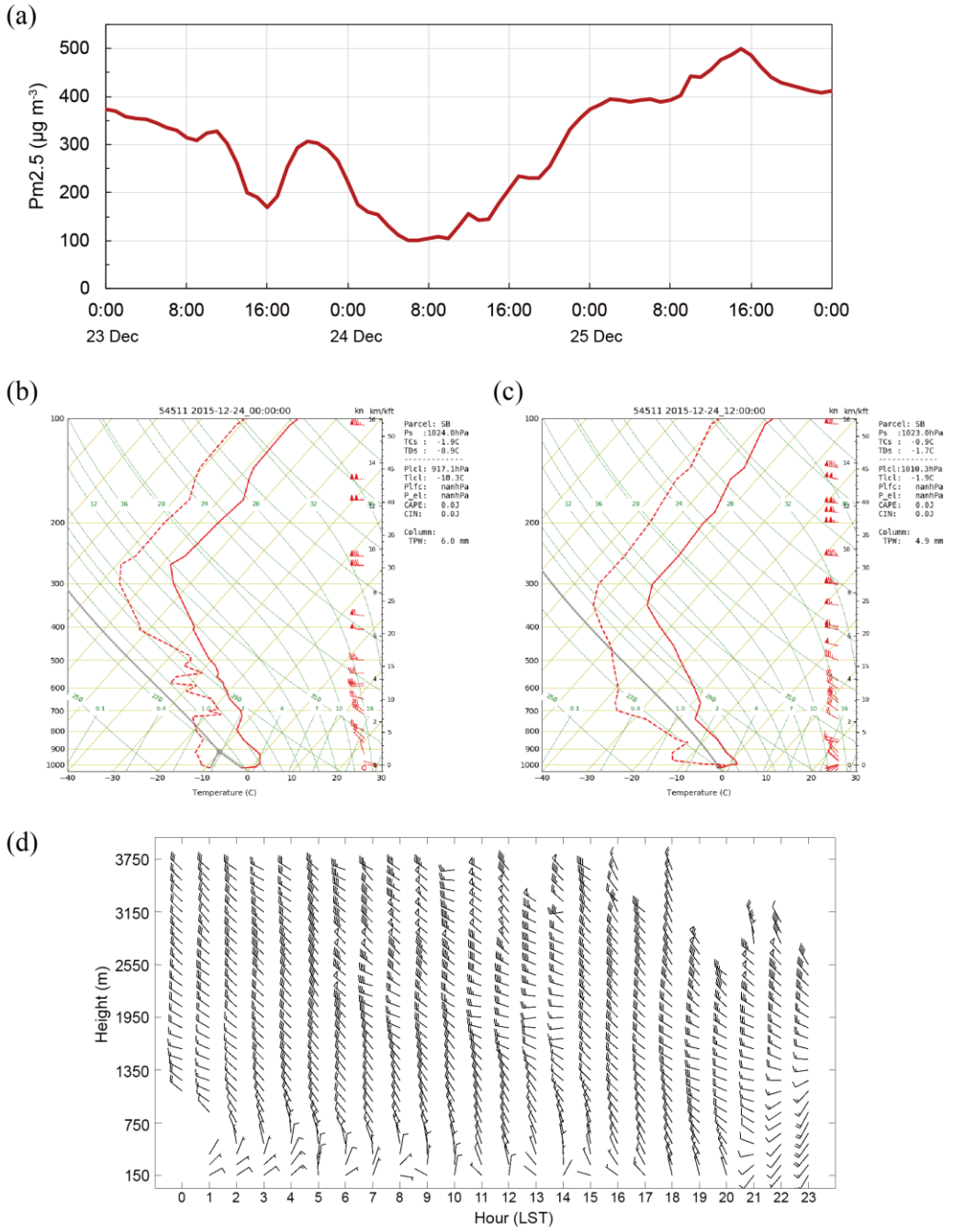

Figure 2. (a) Hourly-mean $PM_{2.5}$ concentration of CP, AOT, YZ and 3-stations mean~~35 air quality stations~~ in Beijing from 23 December to 25 December. Temperature (solid), dew point (dashed), and wind vectors (in knots) from the radio sounding profiles at (b) 00:00 UTC and (c) 12:00 UTC at GXT. (d) The temporal variation of hourly wind-vector profiles from the wind profiler at HD on 24 December 2015.

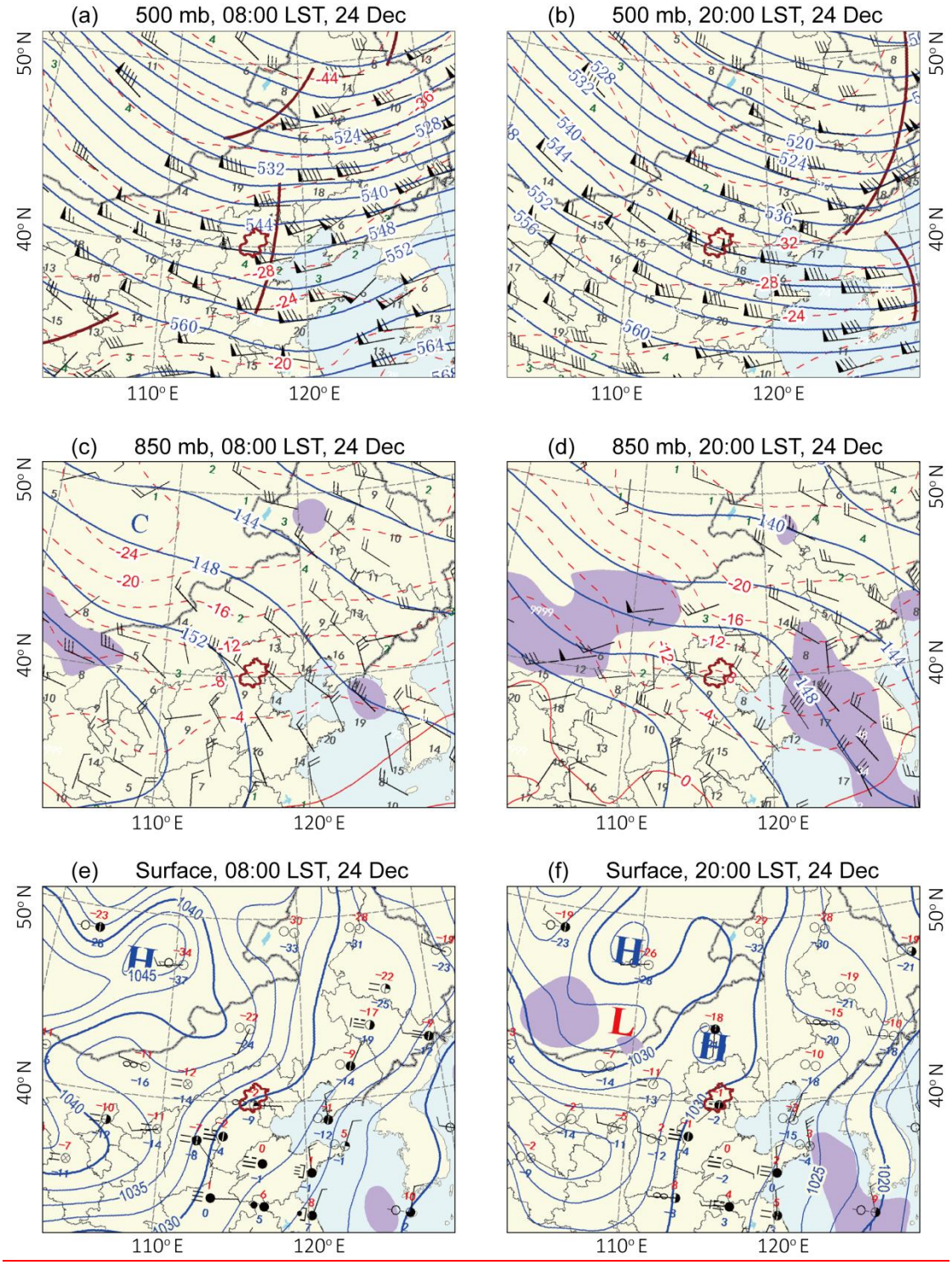
(a) 500 mb, 08:00 LST, 24 Dec
(b) 500 mb, 20:00 LST, 24 Dec
(c) 850 mb, 08:00 LST, 24 Dec
(d) 850 mb, 20:00 LST, 24 Dec
(e) Surface, 08:00 LST, 24 Dec
(f) Surface, 20:00 LST, 24 Dec
50° N
40° N
110° E
120° E
C
H
L

763

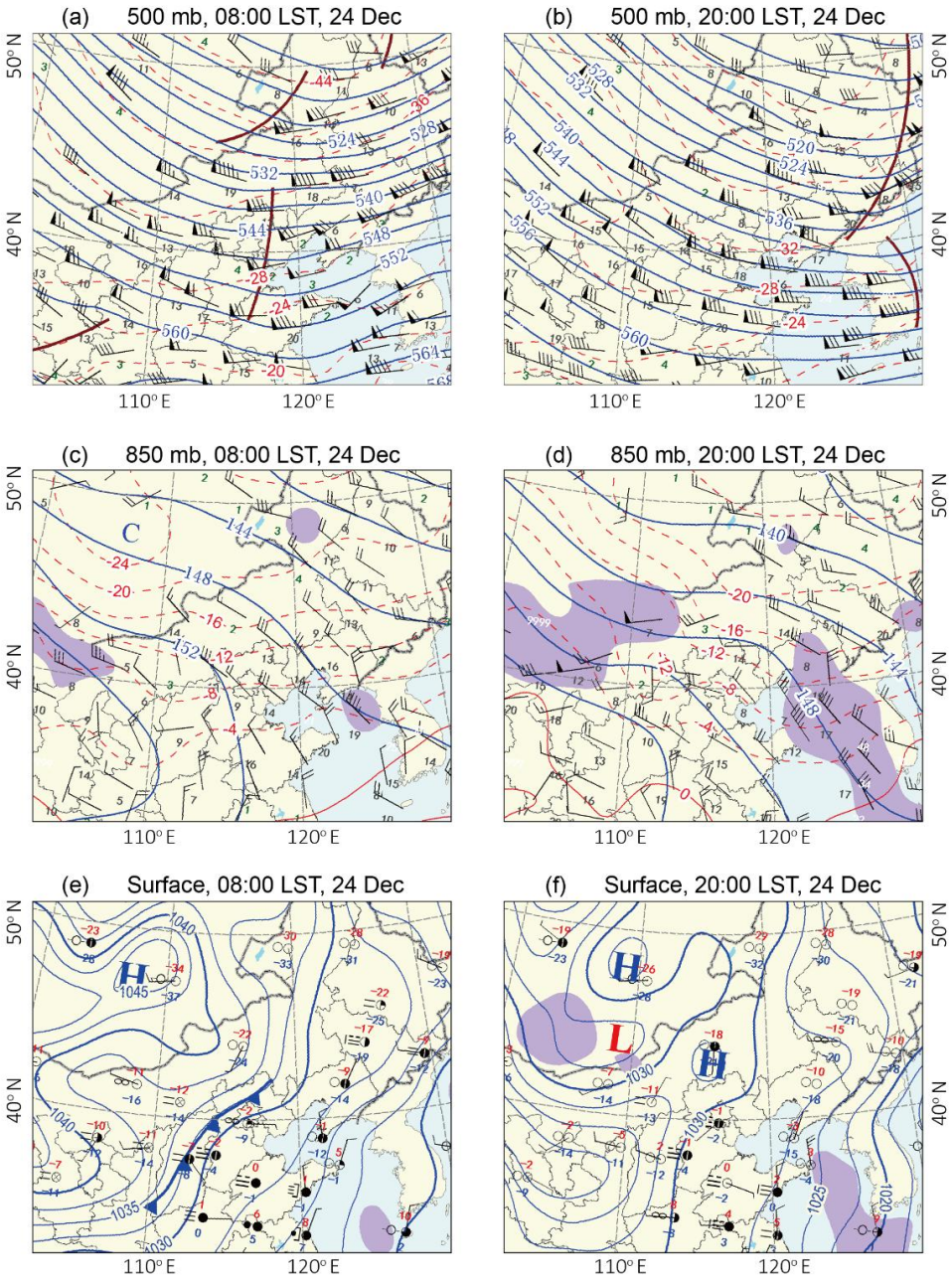

Figure 3. The 500 mb weather maps at (a) 08:00 LST and (b) 20:00 LST, the 8~~0~~50 mb weather maps at (c) 08:00 LST and (d) 20:00 LST, and surface maps at (e) 08:00 LST and (f) 20:00 LST on 24 December 2015. The administrative boundaries of Beijing are marked in brown.

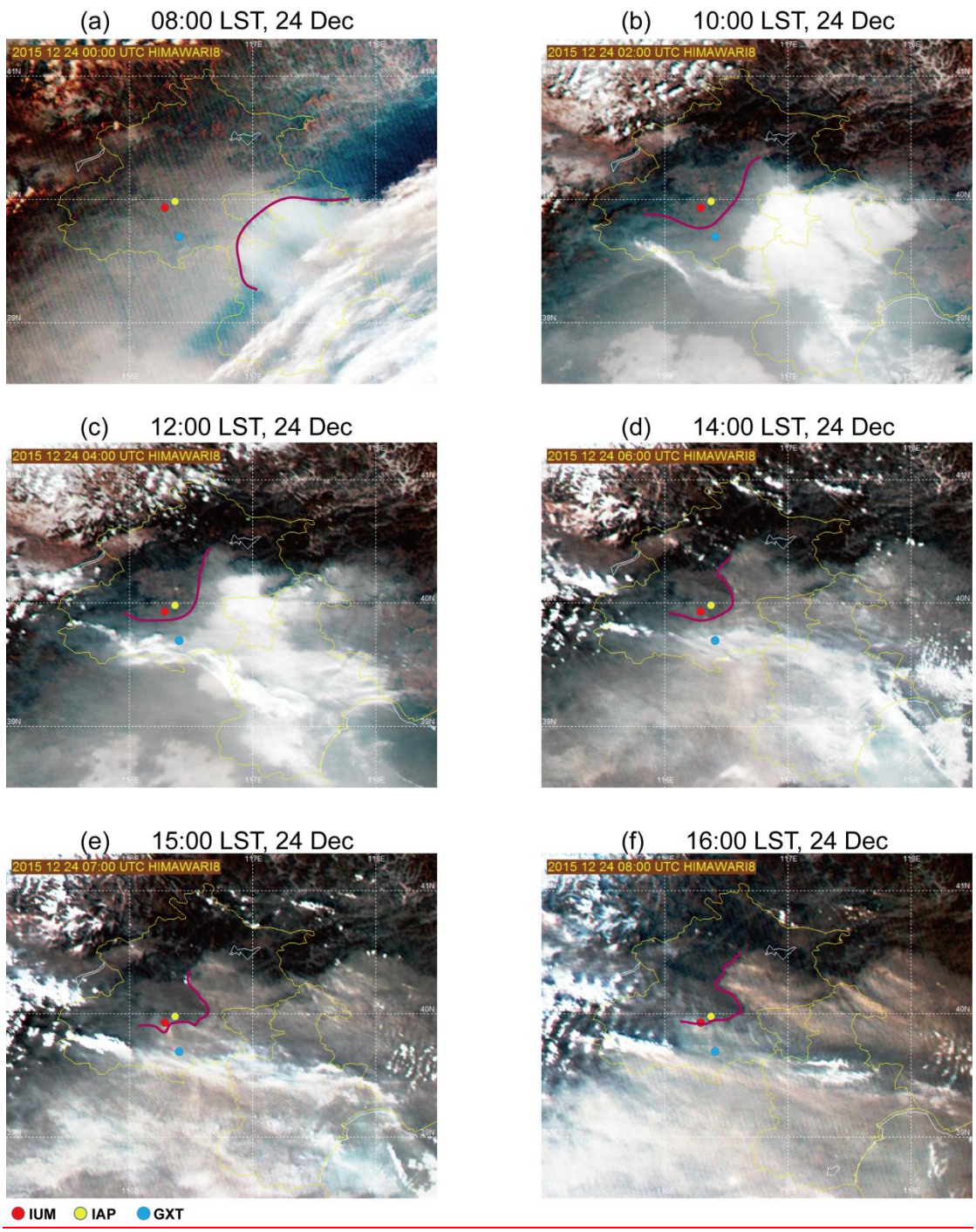
(a) 08:00 LST, 24 Dec
2015 12 24 00:00 UTC HIMAWARI8
(b) 10:00 LST, 24 Dec
2015 12 24 02:00 UTC HIMAWARI8
(c) 12:00 LST, 24 Dec
2015 12 24 04:00 UTC HIMAWARI8
(d) 14:00 LST, 24 Dec
2015 12 24 06:00 UTC HIMAWARI8
(e) 15:00 LST, 24 Dec
2015 12 24 07:00 UTC HIMAWARI8
(f) 16:00 LST, 24 Dec
2015 12 24 08:00 UTC HIMAWARI8
IUM
IAP
GXT

768

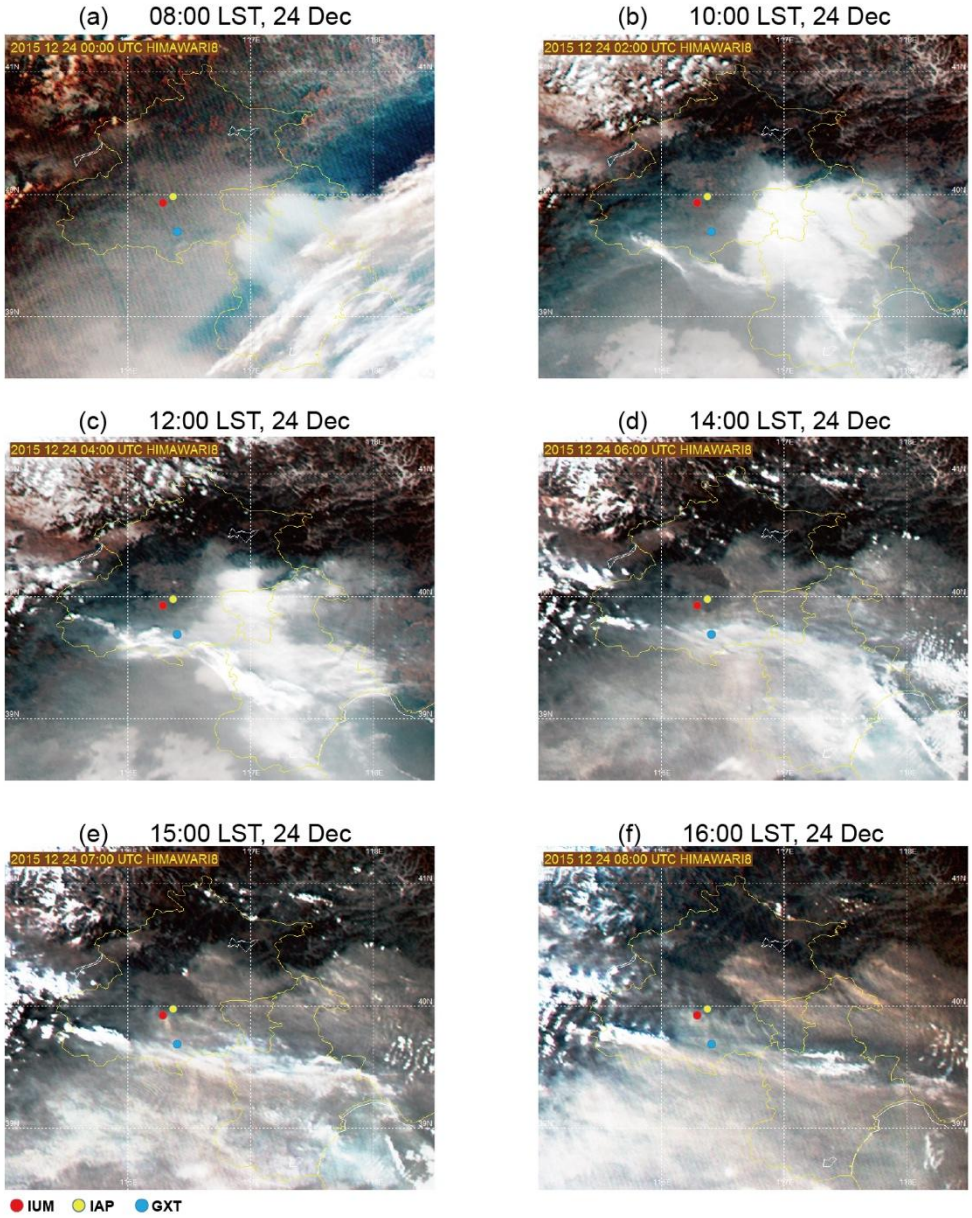

Figure 4. Cloud images from the visible channels of the Himawari satellite at (a) 08:00 LST, (b) 10:00 LST, (c) 12:00 LST, (d) 14:00 LST, (e) 15:00 LST, and (f) 16:00 LST on 24 December 2015. Red, yellow and blue dots are the locations of IUM, IAP and GXT, respectively. The purple lines indicate the location of the haze front.

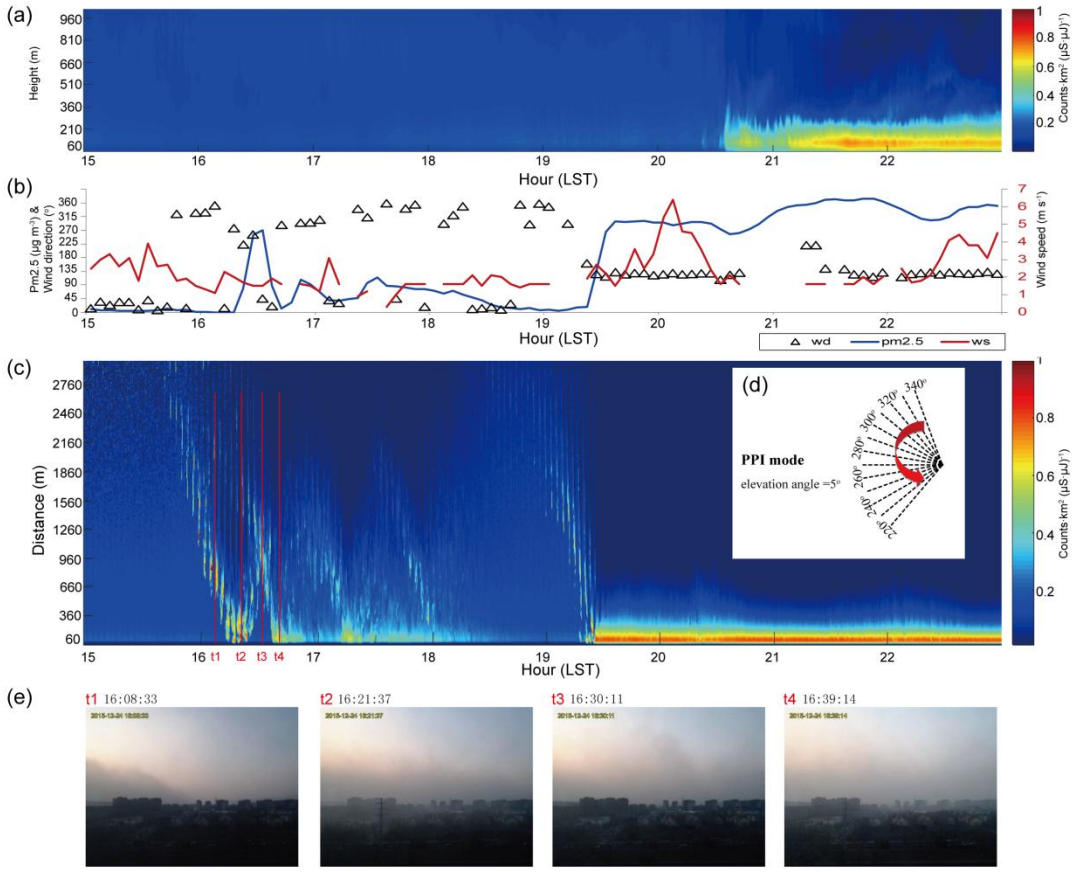
(a)
Height (m)
960
810
660
510
360
210
60
15
16
17
18
19
20
21
22
Hour (LST)
Counts·km² (μS·μJ)⁻¹
1
0.8
0.6
0.4
0.2
(b)
Pm2.5 (μg m⁻³) & Wind direction (°)
360
315
270
225
180
135
90
45
0
Wind speed (m s⁻¹)
7
6
5
4
3
2
1
0
Hour (LST)
wd
pm2.5
ws
(c)
Distance (m)
2760
2460
2160
1860
1560
1260
960
660
360
60
16 t1 t2 t3 t4
Hour (LST)
(d)
PPI mode
elevation angle =5°
340°
320°
300°
280°
260°
240°
220°
(e)
t1 16:08:33
t2 16:21:37
t3 16:30:11
t4 16:39:14

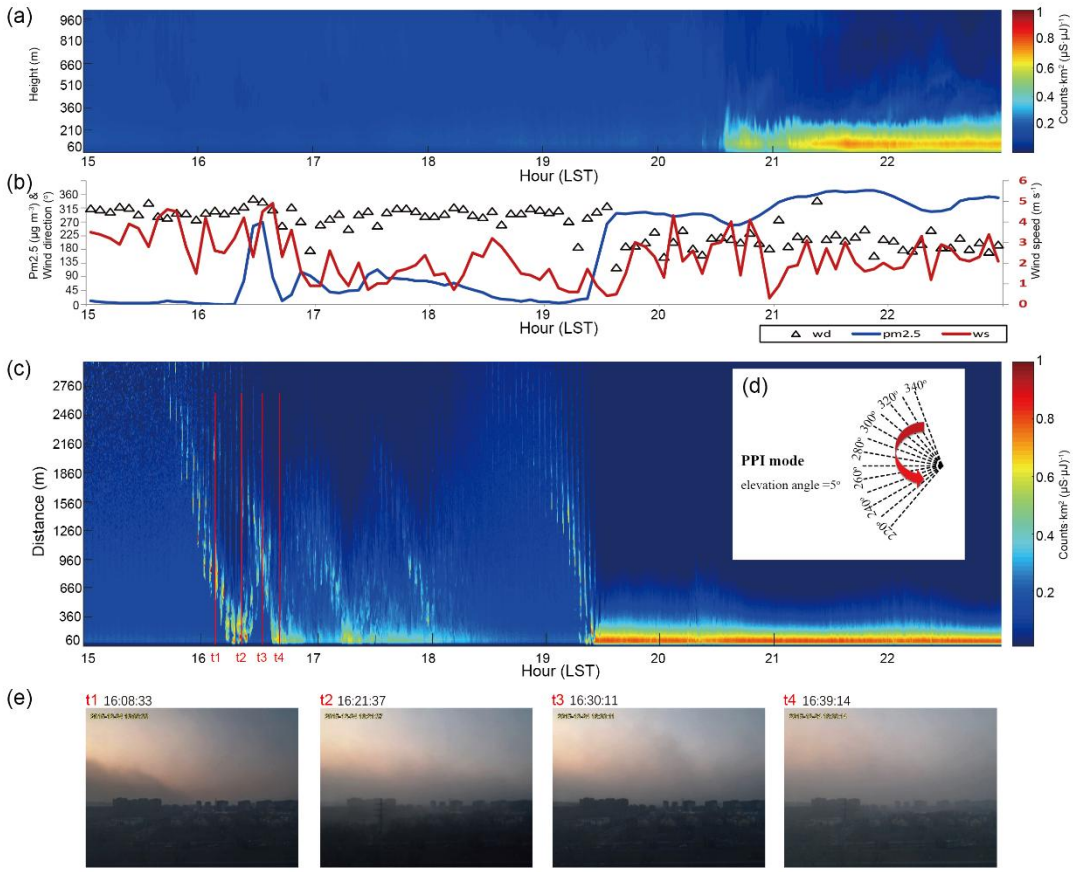

Figure 5. (a) ~~The Min-MPL~~ Vv~~ertical~~ly ~~scanned~~ normalized relative backscatter (NRB) from the Mini-MPL at IAP. (b) 5-min average wind speed (red line), wind direction (triangles) ~~at CDG station~~ and $PM_{2.5}$ concentrations (blue line) at IUM. (c) The NRB from a ~~Min-MPL~~Mini-MPL at ~~IAP~~ IUM scanning in (d) plan position indicator (PPI) mode using 10^{o} horizontal angle intervals from 340^{o} to 220^{o} and at 5^{o} elevation angle. (e) Four photos taken by the weather camera at IUM at times t1, t2, t3 and t4 which are marked as red lines in the upper plot.

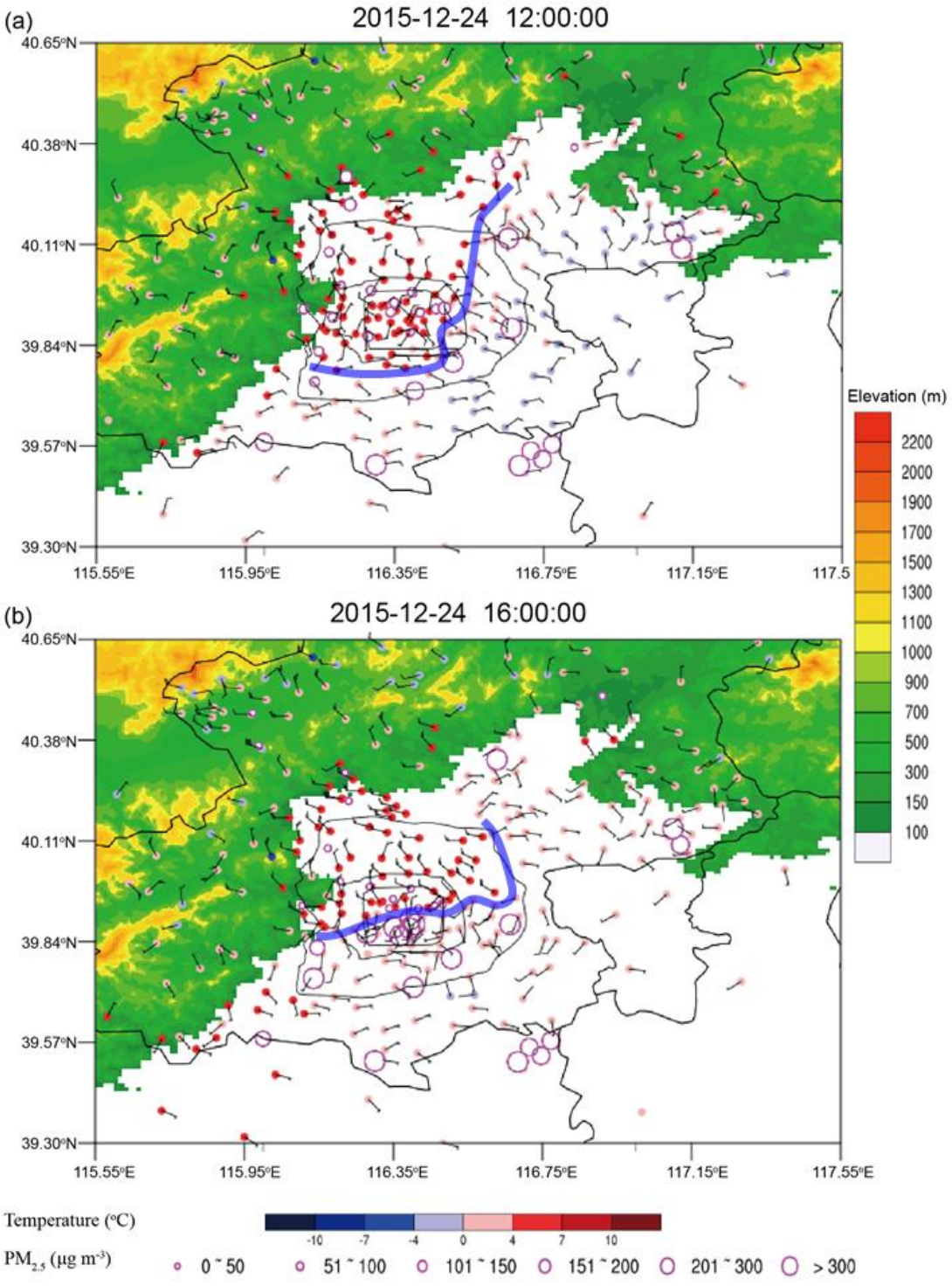

Figure 6. Temperature (color filled dots coded according to the bottom color bar), wind vectors (2 m s^{-1} is one full bar) and $PM_{2.5}$ concentrations (purple circles; the size of the circle represents concentration values) in the plain area within and around Beijing at (a) 12:00 LST and (b) 16:00 LST. The blue lines indicate the location of the haze front.

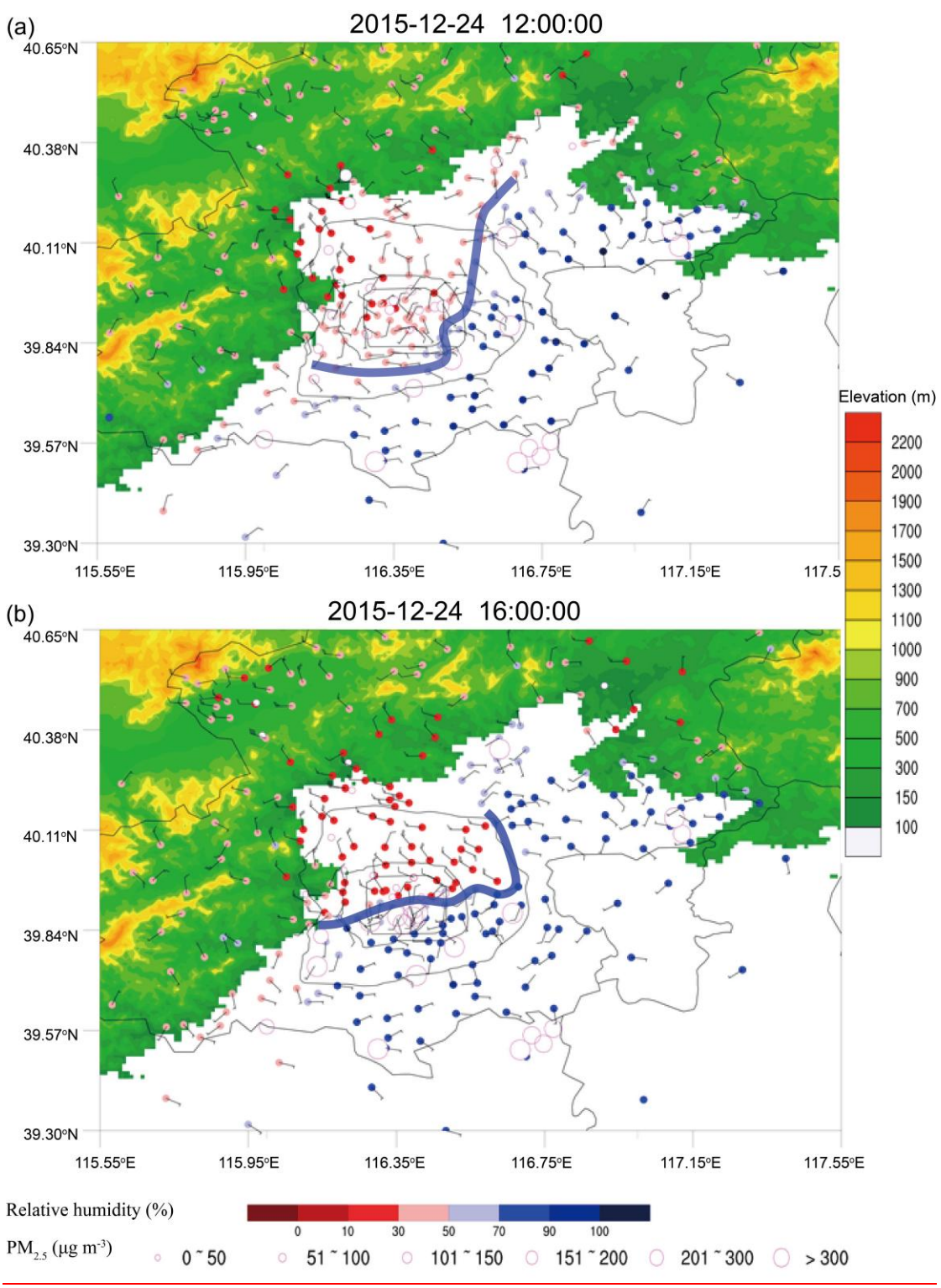
(a)
2015-12-24 12:00:00
40.65°N
40.38°N
40.11°N
39.84°N
39.57°N
39.30°N
115.55°E
115.95°E
116.35°E
116.75°E
117.15°E
117.5
(b)
2015-12-24 16:00:00
40.65°N
40.38°N
40.11°N
39.84°N
39.57°N
39.30°N
115.55°E
115.95°E
116.35°E
116.75°E
117.15°E
117.55°E
Elevation (m)
2200
2000
1900
1700
1500
1300
1100
1000
900
700
500
300
150
100
Relative humidity (%)
0
10
30
50
70
90
100
PM2.5 (μg m-3)
0 ~ 50
51 ~ 100
101 ~ 150
151 ~ 200
201 ~ 300
> 300

792

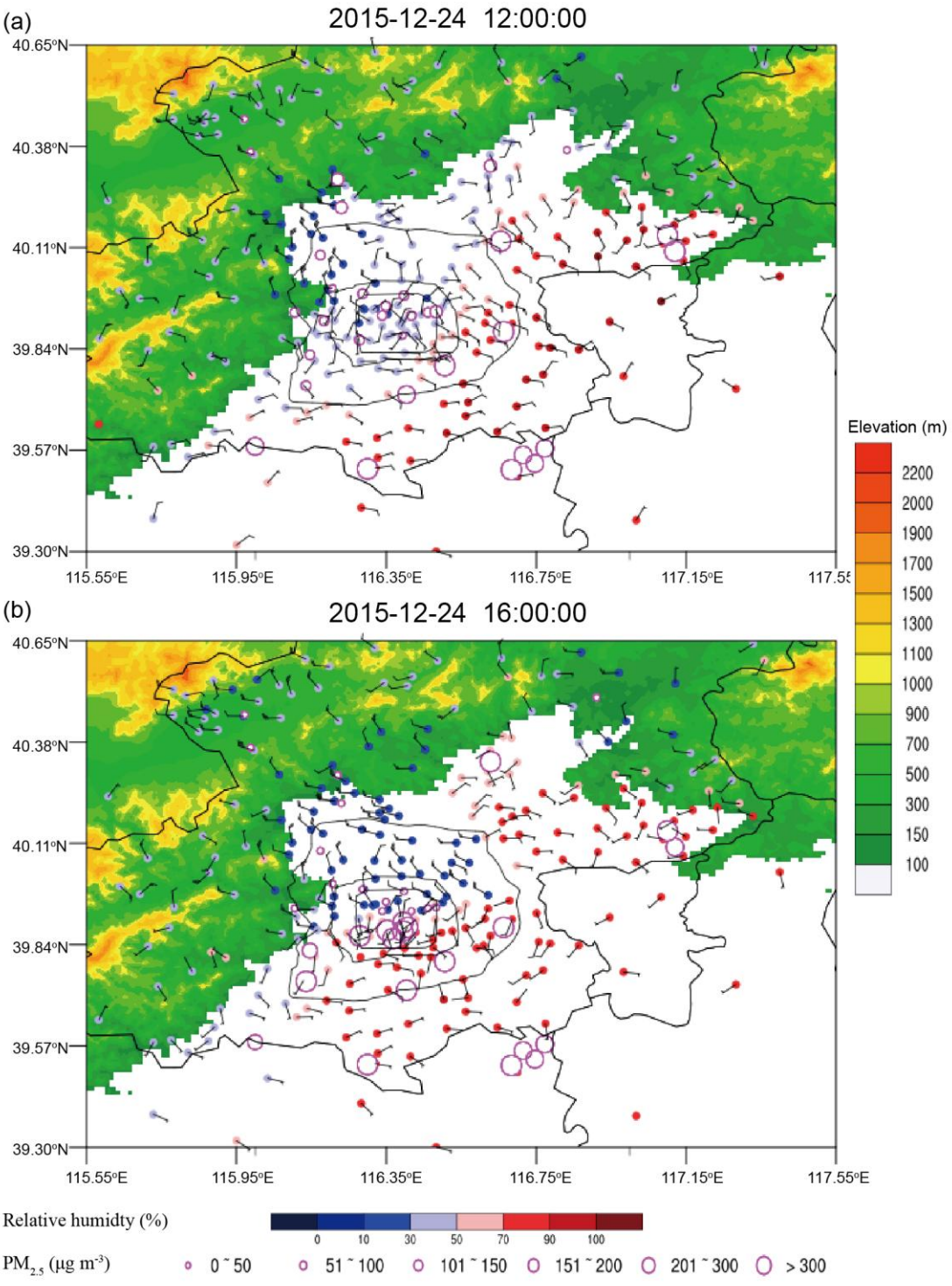

Figure 7. Same as Fig 6, but with relative humidity.

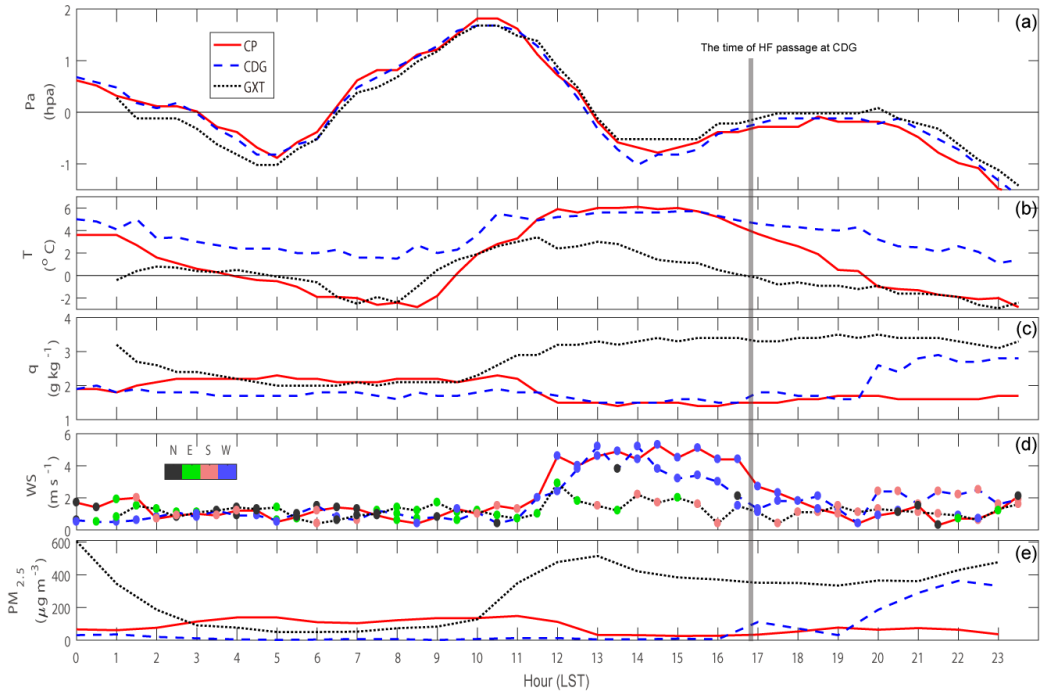

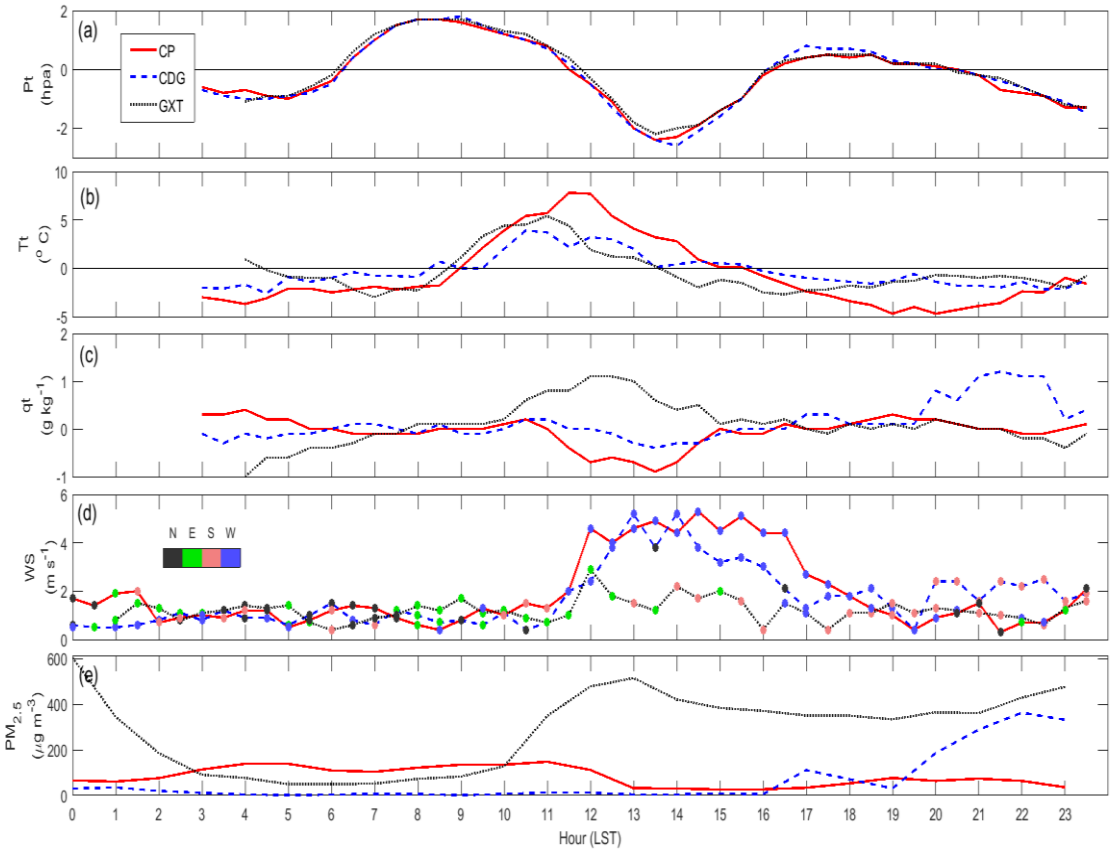

Figure 8. Half-~~Three-h~~hourly (a) pressure anomaly~~tendency~~, (b) air temperature ~~tendency~~, ~~and~~ (c) specific humidity, and (d) wind speed (lines) and wind directions (colored dots), and (e) hourly $PM_{2.5}$ concentration at CP (red line), CDG (blue dash line) and GXT (black dash line) on 24

December 2015. The gray line indicates the time of HF passage at CDG.

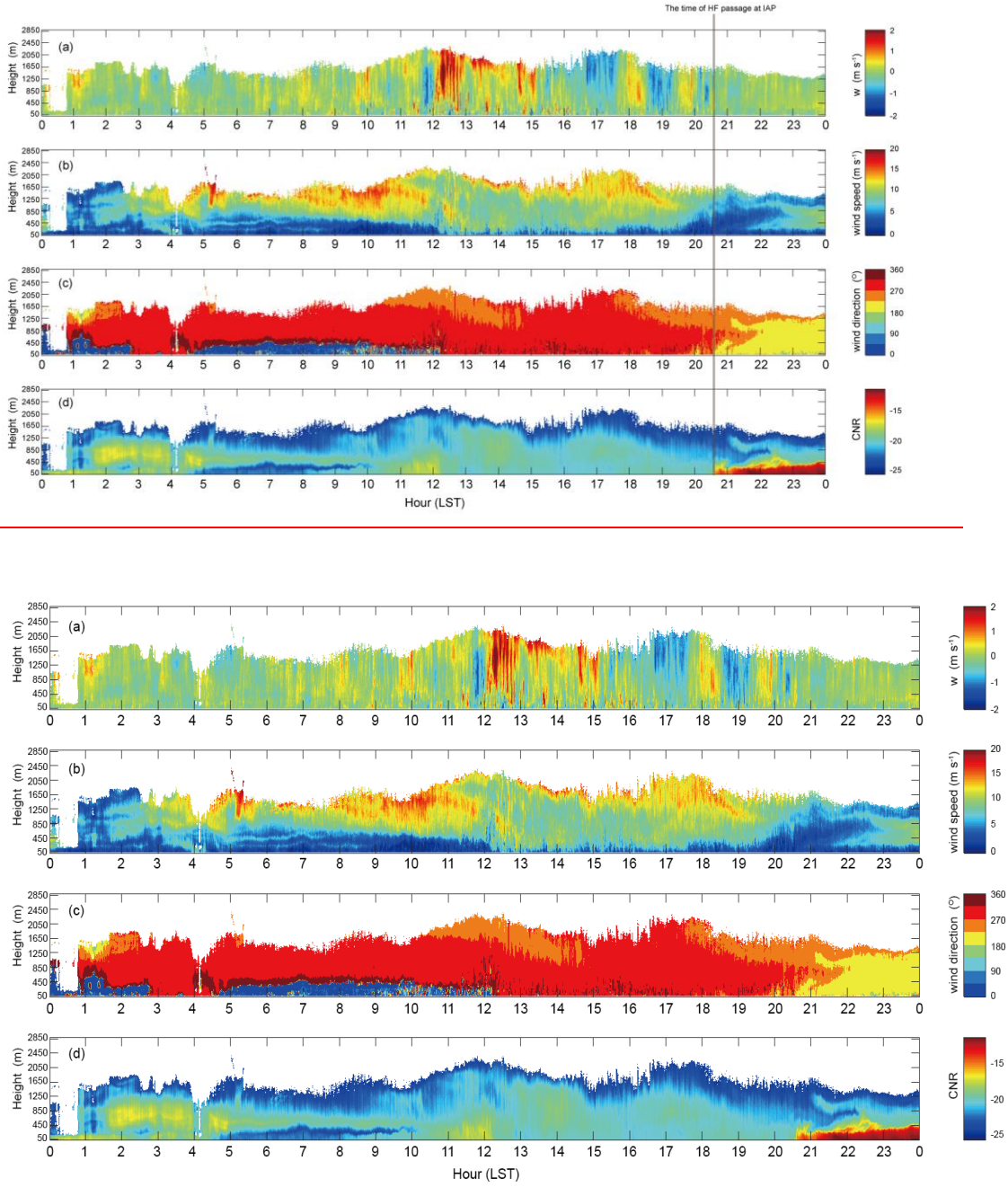

Figure 9. Doppler lidar observations of (a) vertical wind velocity, (b) horizontal wind speed, (c) wind direction, and (d) carrier-noise-ratio (CNR) at IAP on 24 December 2015. The gray line indicates the time of HF passage at IAP.

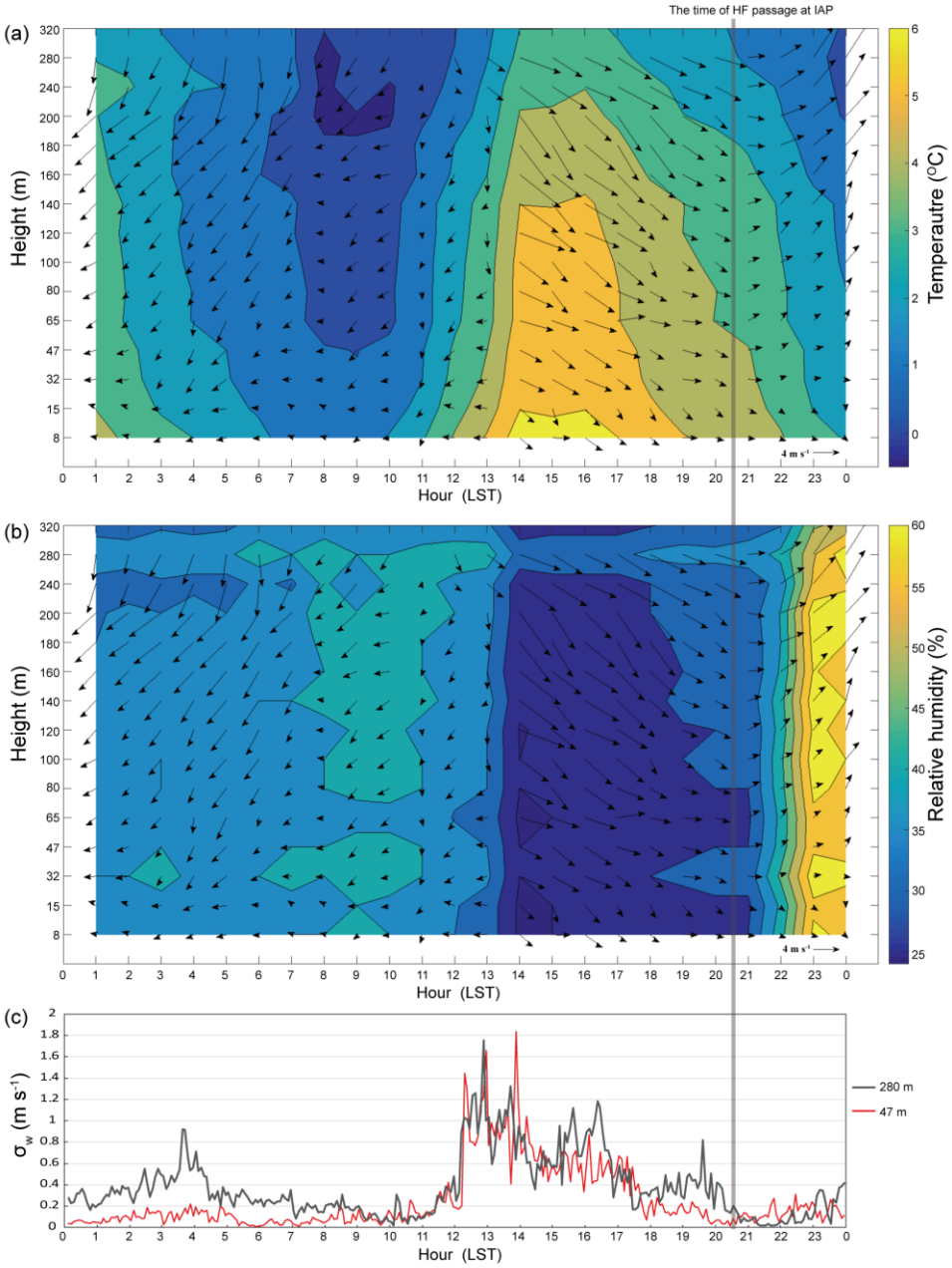
The time of HF passage at IAP
(a)
Height (m)
Hour (LST)
Temperautre (°C)
4 m s⁻¹
(b)
Height (m)
Hour (LST)
Relative humidity (%)
4 m s⁻¹
(c)
σw (m s⁻¹)
Hour (LST)
280 m
47 m

813

814

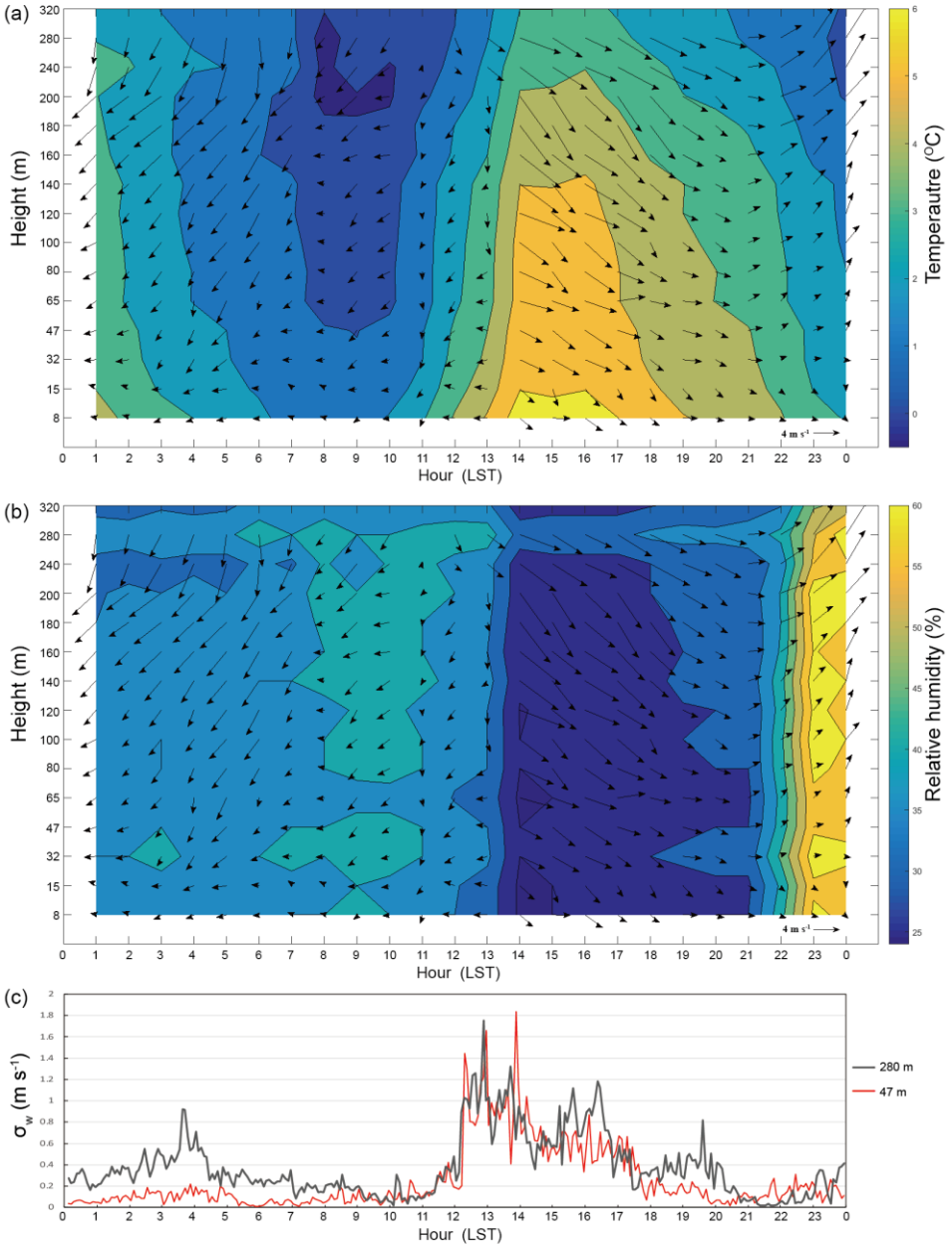

Figure 10. Temporal variations of (a) temperature (colored contours) and wind vectors, (b) relative humidity (colored contours) and wind vectors at 15 levels on the IAP tower, and (c) vertical velocity ~~variance~~ standard deviation at 47 m and 280 m on the IAP tower on 24 December 2015. The gray line indicates the time of HF passage at IAP.

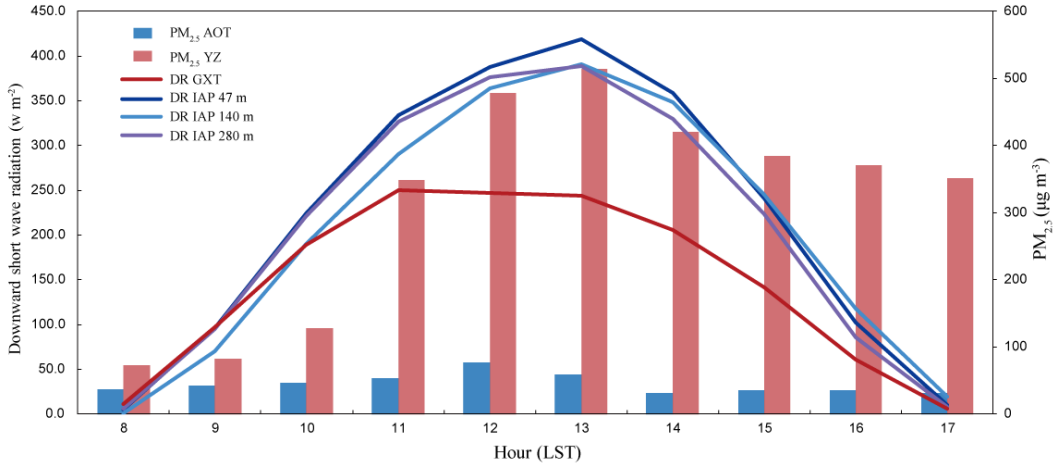

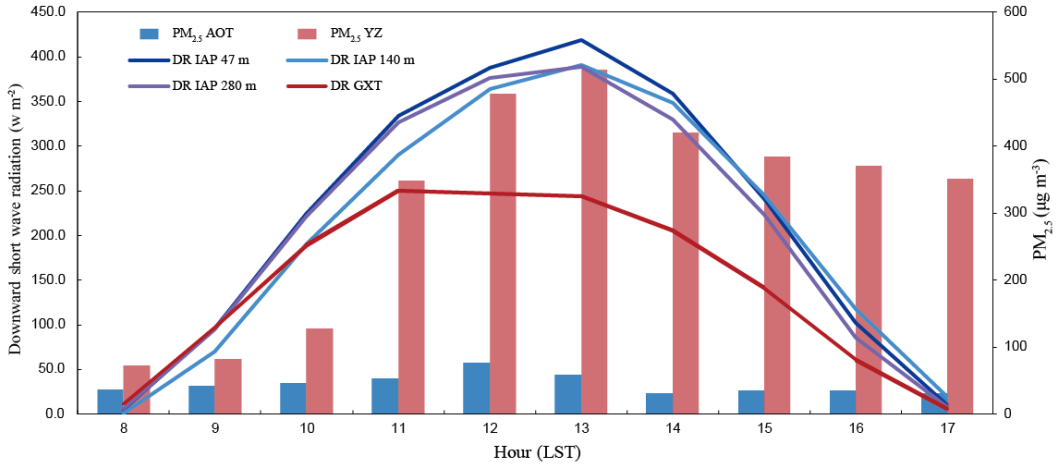

Figure 11. The temporal variations of $PM_{2.5}$ concentrations at ~~ATZX~~AOT (blue bars) and YZ (red bars), and downward short-wave radiation at GXT and at heights of 47 m, 140 m and 280 m on the IAP tower during daytime on 24 December 2015.

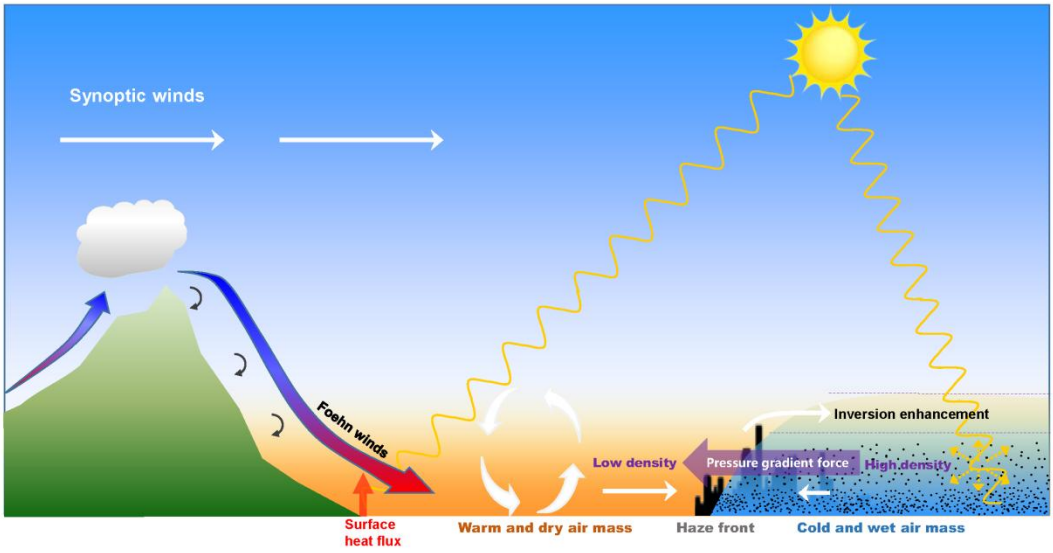

Figure 12. Schematic diagram of the haze front formation.